UNIVERSITY
OF TRENTO

DIPARTIMENTO DI INGEGNERIA E SCIENZA DELL'INFORMAZIONE

38123 Povo – Trento (Italy), Via Sommarive 14
http://www.disi.unitn.it

ON THE EFFECTS OF THE ELECTROMAGNETIC SOURCE MODELLING IN THE ITERATIVE MULTISCALING METHOD

D. Franceschini, M. Donelli, and A. Massa

June 2007

Technical Report # DISI-11-064

On the Effects of the Electromagnetic Source Modeling in the Iterative Multiscaling Method

Davide Franceschini, Massimo Donelli, and Andrea Massa

Department of Information and Communication Technologies,
University of Trento, Via Sommarive 14, 38050 Trento - Italy
Tel. +39 0461 882057, Fax +39 0461 882093
E-mail: *andrea.massa@ing.unitn.it*, {*davide.franceschini*, *massimo.donelli*}*@dit.unitn.it*
Web: *http://www.eledia.ing.unitn.it*

On the Effects of the Electromagnetic Source Modeling in the Iterative Multiscaling Method

Davide Franceschini, Massimo Donelli, and Andrea Massa

Abstract

The validation against experimental data is a fundamental step in the assessment of the effectiveness of a microwave imaging algorithm. It is aimed at pointing out the limitations of the numerical procedure for a successive application in a real environment. Towards this end, this paper evaluates the reconstruction capabilities of the Iterative Multi-Scaling Approach (IMSA) when dealing with experimental data by considering different numerical models of the illuminating setup. In fact, since the incident electromagnetic field is usually collected in a limited set of measurement points and inversion methods based on the use of the "*state*" equation require the knowledge of the radiated field in a finer grid of positions, an effective numerical procedure for the synthesis of the electromagnetic source is generally needed. Consequently, the performances of the inversion process may be strongly affected by the numerical model and, in such a case, a great care should be devoted to this key issue to guarantee suitable and reliable reconstructions.

Keywords:

Microwave Imaging, Inverse Scattering, Iterative Multi-scaling Method, Source Modeling.

Index Terms:

6982 Radio Science: Tomography and imaging; 0629 Electromagnetics: Inverse scattering; 0669 Electromagnetics: Scattering and diffraction.

1 Introduction

Within the framework of the medicine [*Louis*, 1992] and biomedical engineering (see for example [*Liu et al.*, 2003] and the references cited therein), without forgetting the industrial quality control in industrial processes [*Hoole et al.*, 1991] and the subsurface sensing [*Dubey et al.*, 1995; *Daniels*, 1996], many different applications require a non-invasive sensing of inaccessible areas. Towards this end, microwave imaging methodologies [*Steinberg*, 1991] have recently gained a growing attention since they allow to retrieve information on the environment probed with electromagnetic fields by fully exploiting the scattering phenomena [*Colton and Kress*, 1992].

Unfortunately, the inverse problem to be faced is intrinsically nonlinear, ill-posed, and non-unique [*Denisov*, 1999]. In particular, the ill-posedness and the non-uniqueness arise from the limited amount of information collectable during the acquisition of the scattered field. The number of independent scattering data is limited [*Bertero et al.*, 1995; *Bucci and Franceschetti*, 1989] and they can only be used to retrieve a finite number of parameters of the unknown contrast function. To fully exploit such an information and to achieve a suitable resolution accuracy, several multi-resolution strategies have been proposed [*Miller and Willsky*, 1996a, 1996b; *Bucci et al.*, 2000a, 2000b; *Baussard et al.*, 2004a, 2004b].

The Iterative Multi-Scaling Approach belongs to this class of algorithms [*Caorsi et al.*, 2003]. The unknown scatterers are iteratively reconstructed by considering initially a rough estimate of the dielectric distribution[1] and by enhancing successively the spatial resolution in a set of regions-of-interest (RoIs) where the objects have been localized. Such a strategy is mathematically formulated by defining a suitable multi-resolution cost function whose global minimum is assumed as the estimated solution. The functional is iteratively minimized by using a conjugate-gradient-based procedure [*Kleinman and Van den Berg*, 1992], but stochastic [*Massa*, 2002] or hybrid algorithms can be suitably applied.

In order to validate such an approach, the multi-resolution algorithm has been tested against experimental data [*Caorsi et al.*, 2004a] collected in a controlled environment

[1] The IMSA is initialized by considering the free space distribution, then no *a-priori* information on the scenario under test is exploited. Moreover, the initialization of the intermediate steps is obtained from the reconstruction of the previous step with a simple mapping of the retrieved profile in the new discretization of the RoI.

[*Belkebir and Saillard*, 2001], since synthetically-generated data can give only limited indications and they model an ideal scenario.

In dealing with real data, one of the key issue is the modeling of the electromagnetic source or of the related radiated field. In general, the electromagnetic field emitted by the probing system is measured only in the observation domain. However, iterative methods based on "*Data*" and "*State*" equations require the knowledge of the incident field (i.e., the field without the scatterers) generated from the source in the investigation domain. Towards this end, an accurate but simply model (i.e., requiring a reasonable computational burden) of the source should be developed. Complicated numerical models accurately reproduce real data, but they are difficult to be implemented starting from a limited number of samples of the radiated electromagnetic field collected in a portion of the observation domain. On the other hand, a rough model could introduce erroneous constraints to the reconstruction process. Nevertheless, whatever the source model, an effective inversion procedure should be able to reconstruct the scatterer under test with an acceptable accuracy according to its robustness to the noise.

In this framework, to assess the effectiveness and the robustness of the IMSA, the results of a set of experiments, where different models for approximating the illuminating source are considered, will be shown.

The paper is organized as follows. In Section 2, the statement of the inverse problem and the mathematical formulation of the IMSA will be briefly resumed, while in Section 3 the numerical models used to synthesize the probing electromagnetic source will be described. A numerical validation and an exhaustive analysis of the dependence of the reconstruction accuracy on the modeling of the radiated field will be carried out in Section 4 by considering some experimental test cases. Finally, some conclusions will be drawn (Sect. 5).

2 Mathematical Formulation

The inversion procedure will be illustrated referring to a two-dimensional geometry (Figure 1). Let us consider an investigation domain D_I, where an unknown scatterer is supposed to be located. The embedding medium is assumed lossless, non-magnetic, and characterized by a dielectric permittivity ε_0. Such a scenario is illuminated by a set of V incident monochromatic electromagnetic fields $E^v_{inc}(x, y)$, $v = 1, ..., V$, and the corresponding scattered fields $E^v_{scatt}\left(x_{m_{(v)}}, y_{m_{(v)}}\right)$, $v = 1, ..., V$, are available (computed as the difference between the field with E^v_{tot} and without the scatterer E^v_{inc}, $E^v_{scatt} = E^v_{tot} - E^v_{inc}$) in $m_{(v)} = 1, ..., M_{(v)}$, $v = 1, ..., V$, positions belonging to the observation domain D_M. The object is described by a contrast function $\tau(x, y) = \varepsilon_r(x, y) - 1 - j\frac{\sigma(x, y)}{2\pi f \varepsilon_0}$, $(x, y) \in D_I$, $\varepsilon_r(x, y)$ and $\sigma(x, y)$ being the dielectric permittivity and the electric conductivity, respectively.

The arising scattering phenomena are mathematically described through the well-known Lippmann-Schwinger integral equations [*Colton and Kress*, 1992]:

$$E^v_{scatt}(x_{m(v)}, y_{m(v)}) = k_0^2 \int_{D_I} G_{2d}(x_{m(v)}, y_{m(v)}|x', y')\tau(x', y')E^v_{tot}(x', y')dx'dy', \quad \begin{array}{l} m_{(v)} = 1, ..., M_{(v)} \\ v = 1, ..., V \end{array} \qquad (x_{m_{(v)}}, y_{m_{(v)}}) \in D_M \tag{1}$$

(*Data Equation*)

$$E^v_{inc}(x, y) = E^v_{tot}(x, y) - k_0^2 \int_{D_I} G_{2d}(x, y|x', y')\tau(x', y')E^v_{tot}(x', y')dx'dy' \quad (x, y) \in D_I \tag{2}$$

(*State Equation*)

where G_{2d} denotes the Green function of the background medium [*Jones*, 1964]. Since the problem associated with (**??**) is ill-posed (see [*Groetsch*, 1993] and [*Vogel*, 2002]) the system matrix after discretization of the *Data Equation* (according to the Richmond's procedure [*Richmond*, 1965]) is highly ill-conditioned, and, hence the problem is extremely sensitive to the the noise. To remedy this ill-conditioning, a regularization is needed. Thus, the problem is then reformulated in finding the unknown contrast function that minimizes a suitable cost function generally defined as follows

$$\begin{aligned} &\Phi\left\{\tau\left(x_n, y\right), E^v_{tot}\left(x_n, y_n\right); n = 1, ..., N; v = 1, ..., V\right\} = \\ &= \sum_{v=1}^{V} \sum_{m_{(v)}=1}^{M_{(v)}} \left| E^v_{scatt}\left(x_{m_{(v)}}, y_{m_{(v)}}\right) - \sum_{n=1}^{N} \left\{\tau\left(x_n, y_n\right) E^v_{tot}\left(x_n, y_n\right) G^{ext}_{2d}\left(A_n, \rho_{nm_{(v)}}\right)\right\}\right|^2 \\ &+ \sum_{v=1}^{V} \sum_{n=1}^{N} \left| E^v_{inc}\left(x_n, y_n\right) - \left[E^v_{tot}\left(x_n, y_n\right) - \sum_{u=1}^{N} \left\{\tau\left(x_u, y_u\right) E^v_{tot}\left(x_u, y_u\right) G^{int}_{2d}\left(A_u, \rho_{un}\right)\right\}\right]\right|^2 \end{aligned} \tag{3}$$

where G_{2d}^{int} and G_{2d}^{ext} indicate the discretized forms of the internal and external Green's operators [*Colton and Kress*, 1992], $\rho_{nm_{(v)}} = \sqrt{\left(x_n - x_{m_{(v)}}\right)^2 + \left(y_n - y_{m_{(v)}}\right)^2}$, $\rho_{un} = \sqrt{(x_u - x_n)^2 + (y_u - y_n)^2}$ and A_n (A_u) is the area of the n-th (u-th) square discretization domain. In particular, the first term of (**??**) enforces fidelity to the scattered data in the observation domain ($E_{scatt}^v(x_{m_{(v)}}, y_{m_{(v)}})$, $(x_{m_{(v)}}, y_{m_{(v)}}) \in D_M$) and it amounts to the residual error with respect to the scattered field computed from the *Data Equation* (**??**). The second term is a regularization term equal to the residual error with respect to the incident field in the investigation domain ($E_{inc}^v(x_n, y_n)$, $(x_n, y_n) \in D_I$) computed from the *State Equation* (**??**).

However, due to the limited amount of information content in the input data [*Bucci and Franceschetti*, 1989], it would be problematic to parametrize the investigation domain in terms of a large number N of pixel values (in order to achieve a satisfying resolution level in the reconstructed image). To overcome this drawback, an initial uniform (coarse) discretization is used and successively an iterative parametrization of the test domain allows to adaptively increase the resolution level only in the region-of-interest of the investigation area thus achieving the required reconstruction accuracy [*Caorsi et al.*, 2003]. To retrieve the unknown scatterer (i.e., an object function that better fits the problem data, ($E_{scatt}^v(x_{m_{(v)}}, y_{m_{(v)}})$, $E_{inc}^v(x, y)$), Eqs. (**??**) and (**??**) are discretized according to the Richmond's procedure [*Richmond*, 1965]. Moreover, to better exploit the limited information content of the scattering data, an adaptive multi-resolution strategy is adopted [*Caorsi et al.*, 2003].

More in detail, such an adaptive multi-resolution algorithm can be briefly described as follows. Firstly, the IMSA considers ($i = 0$, i being the step index) an homogeneous discretization of the investigation domain with a number of discretization domains $N_{(0)}$ equal to the essential dimension of the scattered data and computed according to the criterion defined in [*Isernia et al.*, 2001]. Then, a "coarse" reconstruction of the investigation domain is yielded by minimizing (**??**) starting from the free-space configuration [$\tau(x_{n_{(0)}}, y_{n_{(0)}}) = 0.0$ and $E_{tot}^v(x_{n_{(0)}}, y_{n_{(0)}}) = E_{inc}^v(x_{n_{(0)}}, y_{n_{(0)}})$] in order to assess the robustness of the overall approach with respect to the "starting guess" in "worst-case". After the minimization, where a set of conjugate-gradient iterations (k being the iteration index) is performed not modifying the discretization grid, a new focused investigation domain (RoI), $D_{O(i)}$, $i = 0$, is defined. Such a squared area is centered at

$$x_{c_{(i)}}^{RoI} = \frac{x_{re_{(i)}}^{RoI} + x_{im_{(i)}}^{RoI}}{2}, \quad y_{c_{(i)}}^{RoI} = \frac{y_{re_{(i)}}^{RoI} + y_{im_{(i)}}^{RoI}}{2} \tag{4}$$

where $x_{re_{(i)}}^{RoI}$, $x_{im_{(i)}}^{RoI}$, $y_{re_{(i)}}^{RoI}$ and $y_{im_{(i)}}^{RoI}$ are defined as

$$x_{\Re(i)}^{RoI} = \frac{\sum_{r=1}^{R} \sum_{n_{(r)}=1}^{N_{(r)}} \left\{ x_{n_{(r)}} \Re\left[\tau\left(x_{n_{(r)}}, y_{n_{(r)}} \right) \right] \right\}}{\sum_{n_{(r)}=1}^{N_{(r)}} \left\{ \Re\left[\tau\left(x_{n_{(r)}}, y_{n_{(r)}} \right) \right] \right\}}, \quad R = i \tag{5}$$

$$y_{\Re(i)}^{RoI} = \frac{\sum_{r=1}^{R} \sum_{n_{(r)}=1}^{N_{(r)}} \left\{ y_{n_{(r)}} \Re\left[\tau\left(x_{n_{(r)}}, y_{n_{(r)}} \right) \right] \right\}}{\sum_{n_{(r)}=1}^{N_{(r)}} \left\{ \Re\left[\tau\left(x_{n_{(r)}}, y_{n_{(r)}} \right) \right] \right\}} \tag{6}$$

and its side $L_{(i)}$ is defined as follows

$$L_{(i)}^{RoI} = \frac{L_{re_{(i)}}^{RoI} + L_{im_{(i)}}^{RoI}}{2} \tag{7}$$

$$L_{\Re(i)}^{RoI} = 2 \frac{\sum_{r=1}^{R} \sum_{n_{(r)}=1}^{N_{(r)}} \left\{ \frac{\rho_{n_{(r)} c_{(i)}} \Re\left[\tau\left(x_{n_{(r)}}, y_{n_{(r)}} \right) \right]}{max_{n_{(r)}=1,..,N_{(r)}} \left\{ \Re\left[\tau\left(x_{n_{(r)}}, y_{n_{(r)}} \right) \right] \right\}} \right\}}{\sum_{r=1}^{R} \sum_{n_{(r)}=1}^{N_{(r)}} \left\{ \frac{\Re\left[\tau\left(x_{n_{(r)}}, y_{n_{(r)}} \right) \right]}{max_{n_{(r)}=1,..,N_{(r)}} \left\{ \Re\left[\tau\left(x_{n_{(r)}}, y_{n_{(r)}} \right) \right] \right\}} \right\}} \tag{8}$$

where $\Re$ stands for the real or the imaginary part and $\rho_{n_{(r)} c_{(i)}} = \sqrt{\left(x_{n_{(r)}} - x_{c_{(i)}}^{RoI} \right)^2 + \left(y_{n_{(r)}} - y_{c_{(i)}}^{RoI} \right)^2}$. Successively, the iterative process starts ($i \rightarrow i + 1$). According to the multi-resolution strategy, an higher resolution level denoted by R ($R = i$) is adopted only for the RoI. $D_{O(i-1)}$ is discretized in $N_{(i)}$ square sub-domain which number is always chosen equal to the essential dimension of the scattered data [*Bucci and Franceschetti*, 1989]. A finer object function profile is then retrieved, starting from the coarser reconstruction achieved at the (*i-1*)-th step, by minimizing the multi-resolution cost function, $\Phi^{(i)}$, defined as follows:

$$\Phi^{(i)}\left\{\tau^{(i)}\left(x_{n_{(r)}},y_{n_{(r)}}\right),\,E_{tot}^{v\,(i)}\left(x_{n_{(r)}},y_{n_{(r)}}\right);\;\begin{array}{c}r=1,...,R=i;\\ n_{(r)}=1,...,N_{(r)};\quad v=1,...,V\end{array}\right\}=$$
$$=\left\{\sum_{v=1}^{V}\sum_{m_{(v)}=1}^{M_{(v)}}\left|E_{scatt}^{v}\left(x_{m_{(v)}},y_{m_{(v)}}\right)-\sum_{r=1}^{R}\sum_{n_{(r)}=1}^{N_{(r)}}\left\{w\left(x_{n_{(r)}},y_{n_{(r)}}\right)\tau^{(i)}\left(x_{n_{(r)}},y_{n_{(r)}}\right)\right.\right.\right.$$
$$\left.\left.\left.E_{tot}^{v\,(i)}\left(x_{n_{(r)}},y_{n_{(r)}}\right)G_{2d}^{ext}\left(A_{n_{(r)}},\rho_{n_{(r)}m_{(v)}}\right)\right\}\right|^{2}\right\}+\left\{\sum_{v=1}^{V}\sum_{r=1}^{R}\sum_{n_{(r)}=1}^{N_{(r)}}\right.$$
$$\left\{w\left(x_{n_{(r)}},y_{n_{(r)}}\right)\left|E_{inc}^{v}\left(x_{n_{(r)}},y_{n_{(r)}}\right)-\left[E_{tot}^{v\,(i)}\left(x_{n_{(r)}},y_{n_{(r)}}\right)\right.\right.\right.$$
$$\left.\left.\left.\left.-\sum_{u_{(r)}=1}^{N_{(r)}}\left\{\tau^{(i)}\left(x_{u_{(r)}},y_{u_{(r)}}\right)\;E_{tot}^{v\,(i)}\left(x_{u_{(r)}},y_{u_{(r)}}\right)G_{2d}^{int}\left(A_{u_{(r)}},\rho_{u_{(r)}n_{(r)}}\right)\right\}\right]\right|\right\}^{2}\right\} \tag{9}$$

where

$$w(x_{n_{(r)}},y_{n_{(r)}})=\begin{cases}0 & if\;\;(x_{n_{(r)}},y_{n_{(r)}})\notin D_{O(i-1)}\\ 1 & if\;\;(x_{n_{(r)}},y_{n_{(r)}})\in D_{O(i-1)}\end{cases}$$

and R indicates the resolution level and $D_{O(i)}$ denotes the area of the RoI defined at the i-th step of the iterative procedure. It should be pointed out that the definition of (**??**) requires not only the knowledge of the available scattered field in the observation domain $[E_{scatt}^{v}\left(x_{m_{(v)}},\,y_{m_{(v)}}\right)=E_{tot}^{v}\left(x_{m_{(v)}},\,y_{m_{(v)}}\right)-E_{inc}^{v}\left(x_{m_{(v)}},\,y_{m_{(v)}}\right),\ \left(x_{m_{(v)}},\,y_{m_{(v)}}\right)\in D_M]$, but also that of the incident field in $D_{O(i)}$ $[E_{inc}^{v}(x_{n_{(r)}},y_{n_{(r)}}),\ (x_{n_{(r)}},y_{n_{(r)}})\in D_{O(i-1)}]$. This latter information is generally not available from measurements [since, in general, only the samples of $E_{inc}^{v}\left(x_{m_{(v)}},\,y_{m_{(v)}}\right)$ other than $E_{tot}^{v}\left(x_{m_{(v)}},\,y_{m_{(v)}}\right)$ are experimentally measured], therefore it should be synthetically generated by means of a suitable model of the electromagnetic source.

The multi-step process continues by computing a new RoI according to (**??**)(**??**) and by estimating a new dielectric distribution through the minimization of the updated version of (**??**) until a "*stationary reconstruction*" is reached [*Caorsi et al.*, 2003] $(i=I_{opt})$. Such a procedure can be extended to multiple-scatterers geometries by considering a suitable clustering procedure [*Caorsi et al.*, 2004b] aimed at defining the number of scatterers Q belonging to the investigation domain and the regions $D_{O(i)}^{(q)}$, $q=1,...,Q$, where the synthetic zoom will be performed at each step of the iterative process.

3 Modeling the Incident Field

The incident field data play a crucial role in the imaging process since the knowledge/availability of $E^v_{inc}(x, y)$ in the investigation domain adds new information. In fact, as it can be noticed in the equation defining the multi-resolution cost function (**??**), it allows to define another constraint (**??**) for the problem solution then reducing the ill-posedness of the inverse problem [*Bertero and Boccacci*, 1998] since such a term can be also considered as a sort of "regularization term". Clearly, an erroneous or imprecise knowledge of the incident field could considerably affect the reliability of the functional and consequently of the overall imaging process since (**??**) controls the minimization procedure. As a matter of fact, in many practical situations, the incident field is only available at the measurement points belonging to the observation domain, $E^v_{inc}\left(x_{m_{(v)}}, y_{m_{(v)}}\right)$, $\left(x_{m_{(v)}}, y_{m_{(v)}}\right) \in D_M$. Such a situation is commonly encountered when dealing with real data because of the complexity and difficulties in collecting reliable and independent measures in a dense grid of points. Hence, to fully exploit the knowledge of the incident field and before facing with the data inversion, it is mandatory to develop a suitable model able to predict the incident field radiated by the actual electromagnetic source in the investigation domain, $E^v_{inc}(x, y)$, $(x, y) \in D_I$. Towards this aim, in the reference literature (see [*Belkebir and Saillard*, 2001] and the references cited therein), different solutions have been proposed. They are mainly based on plane or cylindrical waves expansions, since far-field conditions are usually satisfied. In this paper, such models will be analyzed and a new distributed model will be proposed. More in detail, let us consider

- the ***Plane-Waves Model* (*PW-Model*)** where the incident field is modeled as the superposition of a set of W plane waves

$$E^v_{inc}(x, y) = \sum_{w=1}^{W} A_w \, e^{-jwk_0(x cos\theta_v + y sin\theta_v)} \tag{10}$$

  θ_v being the incident angle, k_0 the free-space propagation constant, and A_w the amplitude of w-*th* wave;

- the ***Concentric-Cylindrical-Waves Model* (*CCW-Model*)** where the radiated field is represented through the superposition of cylindrical waves according to the following expansion

$$E_{inc}^{v}(x,\, y) = \sum_{w=-W}^{W} A_w H_w^{(2)}\left(k_0\rho\right) e^{jw\phi_v} \tag{11}$$

where A_w is an unknown coefficient, $H_w^{(2)}$ indicates the second kind w-*th* order Hankel function, ρ is the distance between the observation point located at $(x,\, y)$ and the phase center of the radiating system where the w-th line source is placed and ϕ_v the corresponding angle;

- the ***Distributed-Cylindrical-Waves Model* (*DCW-Model*)** where the actual source is replaced with a linear array of equally-spaced line-sources, which radiates an electric field given by

$$E_{inc}^{v}(x,\, y) = -\frac{k_0^2}{8\pi f \varepsilon_0} \sum_{w=1}^{W} A\left(x_w,\, y_w\right) H_0^{(2)}\left(k_0\rho_w\right) \tag{12}$$

  where $A(x_w,\, y_w)$ is the unknown coefficient related to the w-*th* element and ρ_w the distance between the observation point and the w-*th* line source.

Such models are completely defined when the set of unknown coefficients, A_w or $A(x_w,\, y_w)$, have been determined. Therefore, the solution of an inverse source problem, where the known terms are the values of the incident field measured in the observation domain $E_{inc}^{v}\left(x_{m_{(v)}},\, y_{m_{(v)}}\right)$, is required. More in detail, the following system has to be solved:

$$\begin{bmatrix} E_{inc}^{v}(x_1,\, y_1) \\ \ldots \\ \ldots \\ E_{inc}^{v}(x_{m_{(v)}},\, y_{m_{(v)}}) \\ \ldots \\ \ldots \\ E_{inc}^{v}(x_{M_{(v)}},\, y_{M_{(v)}}) \end{bmatrix} = \begin{bmatrix} G_{11} & \ldots & G_{1s} & \ldots & G_{1S} \\ \ldots & \ldots & \ldots & \ldots & \ldots \\ \ldots & \ldots & \ldots & \ldots & \ldots \\ G_{m1} & \ldots & G_{ms} & \ldots & G_{mS} \\ \ldots & \ldots & \ldots & \ldots & \ldots \\ \ldots & \ldots & \ldots & \ldots & \ldots \\ G_{M1} & \ldots & G_{Ms} & \ldots & G_{MS} \end{bmatrix} \begin{bmatrix} I_1 \\ \ldots \\ \ldots \\ I_s \\ \ldots \\ \ldots \\ I_S \end{bmatrix} \tag{13}$$

or in a more concise form

$$[\mathbf{E}] = [\mathcal{G}]\, [\mathbf{I}] \tag{14}$$

where (a) for the PW-model $G_{ms} = e^{-jsk_0 d_m}$, $d_m = x_m cos\theta_v + y_m sin\theta_v$, and $I_s = A_s$, $s = 1, ..., S$, $S = W$; (b) for the CCW-model $G_{ms} = H_s^{(2)}(k_0\rho_m) e^{js\phi_v}$, $\rho_m = \sqrt{(x_m - x_{source})^2 + (y_m - y_{source})^2}$, (x_{source}, y_{source}) being the location of the source, and $I_s = A_{s-1-W}$, $s = 1, ..., S$, $S = 2W+1$; (c) for the DCW-model $G_{ms} = -\frac{k_0^2}{8\pi f \varepsilon_0} H_0^{(2)}(k_0\rho_{ms})$, $\rho_{ms} = \sqrt{(x_m - x_s)^2 + (y_m - y_s)^2}$, and $I_s = A(x_s, y_s)$, $s = 1, ..., S$, $S = W$.

Unfortunately, (**??**) involves the limitations typical of an inverse-source problem (see for example, [*Devaney and Sherman*, 1982]). In particular, $[\mathcal{G}]$ is ill-conditioned and the solution is usually non-stable and non-unique. Now, the problem of determining $[\mathbf{I}]$ from the knowledge of the incident field can be recast as the inversion of the linear operator $[\mathcal{G}]$ through the SVD-decomposition [*Natterer*, 1986]

$$[\mathbf{I}] = [\mathcal{G}]^{+} [\mathbf{E}] \tag{15}$$

where

$$[\mathcal{G}]^{+} = [\mathbf{V}] [\Gamma]^{-1} [\mathbf{U}]^{*} \tag{16}$$

and

$$[\Gamma]^{-1} = \begin{bmatrix} 1/\gamma_1 & ... & 0 \\ ... & 1/\gamma_s & ... \\ 0 & ... & 1/\gamma_S \end{bmatrix} \tag{17}$$

Owing of the properties of $[\mathcal{G}]$, the sequence of singular values $\{\gamma_s\}_{s=1}^{S}$ will be decreasing and convergent to zero. Consequently, the solution of equation (**??**) does not continuously depend on problem data and the unavoidable presence of the noise, due to measurement errors as well as to an inaccurate model of the experimental setup, could produce an unreliable source synthesis.

In the next section, an exhaustive numerical analysis will be carried out to assess the robustness of the IMSA against the error in the incident field data and to better understand "how" and "how much" the model of the actual electromagnetic source affects the IMSA performances.

4 Numerical Analysis

In this section, such an assessment will be performed by considering different targets and starting from experimental data. The scattered data refers to the dataset available at the "Institute Fresnel" - Marseille, France". As described in [*Belkebir and Saillard*, 2001; *Testorf and Fiddy*, 2001; *Marklein et al.*, 2001] and sketched in Figure 2, the bistatic radar measurement system consists of an emitting antenna placed at $r_s = 720 \pm 3mm$ from the center of the experimental setup and a receiver which collects equally-spaced $(5°)$ measurements of $E^v_{tot}\left(x_{m_{(v)}}, y_{m_{(v)}}\right)$ and $E^v_{inc}\left(x_{m_{(v)}}, y_{m_{(v)}}\right)$ on a circular investigation domain of radius $r_m = 760 \pm 3mm$. Note the presence of a blind-sector of $\theta_l = 120°$ around the emitting antenna (Figure 2). The scatterers considered in the following experiments are shown in Figs $2(a)$-(c) for reference.

In the first example [Fig. $2(a)$], we will consider the circular dielectric profile ($L_{ref} = 30\,mm$ in diameter) positioned about $30\,mm$ from the center of the experimental setup ($x_{c_{ref}} = 0.0$, $y_{c_{ref}} = -30\,mm$) and characterized by a homogeneous permittivity $\varepsilon_r(x,\, y) = 3.0 \pm 0.3$ [$\tau(x,\, y) = 2.0 \pm 0.3$]. The square investigation domain, $L_{DI} = 30\,cm$ sided, is partitioned in $N = 100$ homogeneous discretization domains and the reconstruction is performed by exploiting all the available measures ($M_{(v)} = 49$, $v = 1, ..., V$) and views ($V = 36$), but using mono-frequency data ($f = 4\,GHz$).

The performances of the IMSA in terms of quantitative as well as qualitative imaging have been assessed considering necessarily the *State Term*[2] during the minimization of the cost function (**??**) and thus introducing the information-content of the incident electric field. To do this, two simple models for the field emitted by the probing antenna have been preliminary taken into account. The first one represents the radiated field with a plane wave ($W = S = 1$) , the other with a cylindrical wave ($W = 0$, $S = 1$). The amplitudes of the modeled incident waves are estimated according to the SVD-based procedure detailed in Sect. 3 starting from the knowledge of the values of the incident field measured in the forward direction and available directly from the experimental dataset. They turn out to be $\left|A^{(PW-Model)}_{w=1}\right| = 1.23$ and $\left|A^{(CCW-Model)}_{w=0}\right| = 17.27$, respectively.

In spite of the inaccuracy in reproducing the values of the incident field collected at the

[2] Some examples of algorithms employing only the Data Term can be found in the special section [*Belkebir and Saillard*, 2001].

measurement points [Figs. 3(a)-(d)], starting from such rough models the IMSA is able to localize the unknown target with a satisfactory degree of accuracy as shown in Fig. 4 and confirmed by the geometric parameters reported in Tab. I.

As far as the single-plane-wave model is concerned, it should be pointed out that the reconstructed contrast[3] is characterized by an average value of the object function equal to $\overline{\tau} = 2.1$, then very close to the actual value of the real target. However, several pixels belonging to the area of the reference profile present a larger object function values $[\tau(x_n, y_n) = 2.5]$ and the retrieved object contour does not accurately reproduce a circular shape.

With respect to the PW model, a better reconstruction is obtained when a little more complex source model (i.e., the single CW-Model) is used as it can be observed in Fig. 4(b) and inferred from the values of the error figures (which quantify the qualitative imaging of the scatterer under test) given in Tab. II and defined as follows

$$\rho^{(q)} = \frac{\sqrt{\left[x_{c_{(I_{opt})}}^{(q)} - x_{c_{ref}}^{(q)}\right]^2 + \left[y_{c_{(I_{opt})}}^{(q)} - y_{c_{ref}}^{(q)}\right]^2}}{\lambda} \quad q = 1, ..., Q_{(I_{opt})} \tag{18}$$

$$\Delta^{(q)} = \left\{\frac{\left|L_{(I_{opt})}^{(q)} - L_{ref}^{(q)}\right|}{L_{ref}^{(q)}}\right\} \times 100 \quad q = 1, ..., Q_{(I_{opt})} \tag{19}$$

where the sub-script "*ref*" refers to the actual profile.

According to the indications drawn from these experiments, which point out that even a rough representation of the incident field significantly benefits the inversion of the scattered field data, the successive procedural step will be aimed at refining the numerical model of the electromagnetic source to further improve the effectiveness of the retrieval process. However, it should be noticed out that using a wrong, even though complex, model might actually degrade the reconstruction, thus great care is needed in defining the most suitable complex model. In order to point out such a concept, the problem has been studied considering the previous scattering geometry, but using numerical "measured" data with a controllable degree of noise. More in detail, the following analysis has been carried out. Different electromagnetic sources have been considered to illuminate the scenario under test (i.e., "*PW-Source*", "*CCW-Source*", and "*DCW-Source*") and

[3] If not specified, the IMSA is used to reconstruct the real part of the object function.

starting from the values of the incident field synthetically computed in the observation domain $E^{v}_{inc}\left(x_{m_{(v)}}, y_{m_{(v)}}\right)$, $\left(x_{m_{(v)}}, y_{m_{(v)}}\right) \in D_M$, various source models (i.e., "*PW-Model*", "*CCW-Model*", and "*DCW-Model*") have been synthesized. Then, a noise characterized by a $SNR = 20\,dB$ has been superimposed to the data and the reconstruction process has been carried out starting from the different source models previously determined. The obtained results in terms of qualitative (??)-(??) and quantitative error figures $\xi_{(j)}$defined as

$$\xi_{(j)} = \sum_{r=1}^{R} \frac{1}{N_{(r)}^{(j)}} \sum_{n_{(r)}=1}^{N_{(r)}^{(j)}} \left\{ \frac{\tau(x_{n_{(r)}}, y_{n_{(r)}}) - \tau^{ref}(x_{n_{(r)}}, y_{n_{(r)}})}{\tau^{ref}(x_{n_{(r)}}, y_{n_{(r)}})} \right\} \times 100 \qquad R = S_{opt} \qquad (20)$$

where $N_{(r)}^{(j)}$ can range over the whole investigation domain ($j \Rightarrow tot$), or over the area where the actual scatterer is located ($j \Rightarrow int$), or over the background belonging to the investigation domain ($j \Rightarrow ext$), are reported in Tab. III. As expected, the use of a model corresponding to the actual source turns out to be the most suitable choice and more complex modeling cause larger errors. As an example, let us consider the *PW-source*. When the profile retrieval is performed using the *PW-model* then the reconstruction error is equal to $\xi_{tot} = 0.30$. Otherwise, $\xi_{tot}^{(DCW-Model)} = 13.30$ and $\xi_{tot}^{(CCW-Model)} = 20.53$. Similar conclusions hold true also for other illuminations and source models in terms of quantitative error figures, as well.

Consequently, the more complex source configurations described in Section 3, which consider the superposition of plane waves or of cylindrical waves, have been taken into account in order to define the most suitable source model. In such a framework since the numerical description of the actual source in the real measurement setup is only partially or not generally available, the optimal model has to be defined by looking for the most suitable number of the unknown source coefficients, S, and corresponding values, A_s, $s = 1, ..., S$. For each of the source models, S has been chosen by looking for the configuration that provides a satisfactory matching between measured and numerically-computed values of the incident field in the observation domain. Such a matching has been evaluated by computing the following parameter

$$\mu = (VM_{(v)})^{-1} \sum_{v=1}^{V} \sum_{m_{(v)}=1}^{M_{(v)}} \left\{ \left[Re\left\{ E_{inc}^{v}\left(x_{m_{(v)}}, y_{m_{(v)}}\right)\right\} - Re\left\{ \widetilde{E_{inc}^{v}}\left(x_{m_{(v)}}, y_{m_{(v)}}\right)\right\}\right]^2 + \left[Im\left\{ E_{inc}^{v}\left(x_{m_{(v)}}, y_{m_{(v)}}\right)\right\} - Im\left\{ \widetilde{E_{inc}^{v}}\left(x_{m_{(v)}}, y_{m_{(v)}}\right)\right\}\right]^2 \right\}^{\frac{1}{2}} \tag{21}$$

where $Re\{\cdot\}$ and $Im\{\cdot\}$ stand for the real and imaginary part, respectively, and the super-script ~ indicates a numerically-estimated quantity.

In Fig. 5, the behavior of the "matching parameter" is displayed for different source models. As can be observed, μ reduces when S increases. Thus, the optimal number of source coefficients, S_{opt}, has been heuristically-defined as the value belonging to a stability region. Consequently, the optimal values have been set to: $S_{opt}^{(PW-Model)} = 20$ (where $\mu \simeq 4 \times 10^{-4}$) and $S_{opt}^{(CCW-Model)} = 11$ (where $\mu \simeq 10^{-4}$). The amplitudes of the weighting source coefficients are shown in Fig. 6. The magnitudes of the *CCW-Model* coefficients [Fig. 6(b)] are very large when compared to those of the single *PW-Model* or single *CCW-Model*. As expected, the corresponding radiated-field distributions inside the investigation domain D_I [Figs. 7(c),(d)] turn out to be unacceptable (for comparison purposes, the plot of the incident electric field computed by means of the single *CCW-Model* is given in Figs. 7(e),(f)). Moreover, Figs. 7(a),(b) show how even the incident field synthesized by means of the *PW-Model* presents rather high values with respect to the distribution of Figs. 7(e),(f). Since the incident field is the guess value for the optimization of the internal field, a completely wrong starting distribution may considerably affect the whole retrieval procedure. Accordingly, the adopted inversion strategy is not able to correctly estimate neither the shape nor the dielectric distribution of the unknown scatterer (Fig. 8). As far as the case related to the *PW-Model* is concerned, it should be noted that the iterative process is stopped at the fourth step (Tab. I) and the quality of the reconstructed profile (Fig. 8(a)) turns out to be strongly reduced (if compared to that of Fig. 4(a)) in terms of qualitative as well as quantitative imaging. Similar indications can be drawn from the analysis of the retrieved distribution obtained with the *CCW-Model*. However, reducing the number of terms in the expansion could lead to better results like, for example, those presented in the special section [*Belkebir and Saillard*, 2001] and those obtained in this work by using S=1. Notwithstanding this, the value suggested by the indicator has been used in the proposed experiments.

The obtained discouraging results can be properly motivated by observing the singular-values spectrum (Fig. 9) and by computing the condition number η of the linear matrix operator $[\mathcal{G}]$ (defined as follows $\eta = \frac{max_p\{\sigma_p\}}{min_p\{\sigma_p\}}$), which clearly point out an intrinsic instability of the system and the ill-conditioning of the problem. In more detail, the ill-conditioning index turns out to be equal to $\eta^{(PW-Model)} = 41.07$ and to $\eta^{(CCW-Model)} = 5.62 \times 10^7$, respectively.

A possible solution for suitably defining the source model and, consequently, for improving the resolution accuracy of the retrieval process (alternative to employ a truncated-SVD regularization algorithm as suggested by the step-like behavior of the singular-values spectrum), is to define a spatially-distributed line-source model as described in Sect. 3.

According to the procedure for choosing the number as well as the magnitude of the source weights previously described, a reasonable configuration is $S_{opt}^{(DCW-Model)} = 15$ (Fig. 5) with the coefficients distributed as shown in Fig. 10(a). For completeness, in order to give an idea of the fitting between measured and computed data, Figs. 10(b)-(c) display the values of the amplitude and phase of the radiated-field computed in the observation domain. Moreover, Fig. 11 gives a gray-level representation of the incident electric field synthesized in the investigation domain.

The use of such a model for the incident field allows a significant improvement in the reconstruction. Such a result can be appreciated in Fig. 12 where the gray-level representation of the object function is given. In particular, for this representative configuration, also the intermediate reconstructions [Figs. 12(a)-(c)] of the multi-scaling process are reported in order to show how the profile improves during the iterative procedure. As it can be noticed, even though the computational domain is not finely discretized at the fist step [Fig. 12(a)], the IMSA iteratively increases the resolution in the RoI in order to obtain an accurate discretization at the convergence step [Fig. 12(c)] where a meaningful profile is obtained. As a matter of fact, the localization as well as the dimensioning error of the convergence step [Fig 12(c)] reduces with respect to the other source models ($\rho^{(DCW-Model)} = 0.045\lambda_0$, $\Delta^{(DCW-Model)} \approx 9$ - Tab. II) and the homogeneity of the actual scatterer is better reproduced. As far as the explanation of the better performance of such an approach with respect to the other source-synthesis modalities is concerned, it is mainly motivated by the faithful and stable reproduction [Figs. 10(b)-(c)] of the actual values of the field measured in the observation domain.

To further assess the robustness and the effectiveness of the IMSA, by validating the radiated-field synthesis as well, the second example considers a multiple-scatterers scenario (*"twodielTM_8f.exp"* - [*Belkebir and Saillard*, 2001]). Under the same assumptions of the previous example in terms of measures, radiation frequency, and views as well as extension and partitioning of the investigation domain, two dielectric ($\tau^{(q)} = 2.0 \pm 0.3$, $q = 1, ..., Q$, $Q = 2$) circular ($L_{ref}^{(q)} = 30\,mm$ in diameter) cylinders are placed $90\,mm$ from each other [Fig. 2(b)].

Fig. 13 shows the results of the reconstruction process in correspondence with different source models. As can be seen, whatever the stable source synthesis the two targets are correctly located and dimensioned with a satisfactory accuracy. Certainly, the more sophisticated synthesis approach (*DCW-Model* - $S = 15$) allows to obtain a better reconstruction as confirmed by the geometric parameters of the retrieved profiles resumed in Tab. IV. In order to show the capabilities of the IMSA in estimating the lossless nature of the dielectric scatterers, the reconstruction corresponding to the *DCW-Model* has been run using a blind inversion scheme, that is without a-priori information of its characteristics. Such assumption does not exploit the alternative definition of the solution space, which allows to reconstruct only the real part of the object function. Accordingly, Fig. 13(d) points out that the minimum of the imaginary part of the object function is 0.08 (corresponding to $\sigma = 1.78 \times 10^{-3}\,\frac{S}{m}$).

Finally, in order to complete the validation of the approach, the last example deals with a metallic structure. The scatterer is an U-shaped metallic cylinder [Fig. 2(c)] and the reconstruction is performed starting from the complete data collection of the dataset *"uTM_shaped.exp"* [*Belkebir and Saillard*, 2001] at the working frequency of $f = 4\,GHz$. According to the strategy proposed in [*Van den Berg et al.*, 1995], only the imaginary part of the object function has been retrieved considering a lower bound in the reconstructed contrast and if at some iteration the estimated $Im\{\tau(x, y)\}$ is lower than $\tau_{Im}^{max} = -15.0$, then the contrast is replaced by τ_{Im}^{max}. As a result, the imaginary part of the retrieved profile in the configuration with the *DCW-Model* for the synthesis of the radiated field, is depicted in Fig. 14. At the convergence step ($I_{opt} = 4$), the reconstruction clearly reveals that we are dealing with a U-shaped target. The outer and the inner contour of the "U" are well reproduced (even though little artifacts appear) confirming the effectiveness of approach in shaping and locating dielectric as well metallic scatterers.

5 Conclusions

The Iterative Multi-Scaling Approach has been tested against experimentally-acquired data by focusing the attention on its robustness as regards different mathematical models used to synthesize the incident electric field. The effectiveness of the iterative minimization of the cost functional in reconstructing unknowns scatterers presents a certain degree of sensitivity to the model of the incident field used to formalize the constraint stated by the *State Equation*. By considering a more complex approximation model (*DCM-Model*), satisfactory localizations and reconstructions have been carried out by indicating the positive effect of a suitable synthesis methodology on the inversion process.

However, even though an accurate approximation model generally might result in a more accurate reconstruction, which complex model is more appropriate for the incident field may depend on the measurement setup, especially the microwave source configuration. For example, for simple plane-wave incident field, using the PW-model might reduce artifacts which result from measurement noise. So future investigations are needed by considering other experimental datasets (currently not-available, but under development) to generalize the conclusions of such an analysis.

Moreover, the results of the numerical analysis carried out in the paper and the comparison with the reconstructions obtained in the related literature suggest that improved imaging techniques (e. g., multi-frequency techniques) or additional regularization terms may probably diminish the impact of the incident field model. Since this point has not directly investigated other researches will be aimed at further improving the effectiveness of the IMSA by considering multi-frequency strategies, further regularization terms and more effective optimization algorithms for the minimization of the multi-resolution cost function in order to verify the above hypothesis.

References

Baussard, A., E. L. Miller, and D. Lesselier (2004a), Adaptive multiscale approach for 2D microwave tomography, *URSI - International Symposium on Electromagnetic Theory*, Pisa, Italia, pp. 1092-1094.

Baussard, A., E. L. Miller, and D. Lesselier (2004b), Adaptive multiscale reconstruction of buried objects, *Inverse Problems*, *20*, S1-S15.

Belkebir, K., and M. Saillard (2001), Special section: "Testing Inversion Algorithms against Experimental Data," *Inverse Problems*, *17*, 1565-1702.

Bertero, M., C. De Mol, and E. R. Pike (1995), "Linear inverse problems with discrete data. I: General formulation and singular system analysis," *Inverse Problems*, *1*, 301-330.

Bertero, M., and P. Boccacci (1998), *Introduction to Inverse Problem in Imaging,* IoP Publishing, Philadelphia.

Bucci, O. M., and G. Franceschetti (1989), "On the Degrees of Freedom of Scattered Fields," *IEEE Trans. Antennas Propagat., 37*, 918-926.

Bucci, O. M., L. Crocco, T. Isernia, and V. Pascazio (2000a), Wavelets in non-linear inverse scattering," *Proc. IEEE Geoscience and Remote Sensing Symp.*, IGARSS-2000, *7*, 3130-3132.

Bucci, O. M., L. Crocco, and T. Isernia (2000b), An adaptive wavelet-based approach for non destructive evaluation applications, *Proc. IEEE Antennas Propagation Symp.*, APS-2000, *3*, 1756-1759.

Caorsi, S., M. Donelli, D. Franceschini, and A. Massa (2003), A new methodology based on an iterative multi-scaling for microwave imaging, *IEEE Trans. Microwave Theory Tech.*, *51*, 1162-1173.

Caorsi, S., M. Donelli, and A. Massa (2004a), Analysis of the stability and robustness of the iterative multiscaling approach for microwave imaging applications, *Radio Sci.*, *39*, 1-17.

Caorsi, S., M. Donelli, and A. Massa (2004b), Location, detection, and imaging of multiple scatterers by means of the iterative multiscaling method, *IEEE Trans. Microwave*

Theory Tech., *52*, 1217-1228.

Colton, D., and R. Krees (1992), *Inverse acoustics and electromagnetic scattering theory,* Berlin, Germany: Springer-Verlag.

Daniels, D. J. (1996), "Surface penetrating radar," *IEE Electron. Comm. Eng. J., 8*, 165-182.

Denisov, A. M. (1999), *Elements of theory of inverse problems,* Utrecht, The Netherlands: VSP.

Devaney, A. J., and G. C. Sherman (1982), Nonuniqueness in inverse source and scattering problems, *IEEE Trans. Antennas Propagat.*, *33*, 1034-1037.

Dubey, A. C. (1995), *Detection technology for mines and minelike targets*, Eds. Orlando, FL.

Groetsch, C. W. (1993), *Inverse Problems in Mathematical Sciences,* Wiesbaden, Germany: Vieweg.

Hoole, S. R. H. (1991), Inverse problem methodology and finite elements in the identifications of cracks, sources, materials, and their geometry in inaccessible locations, *IEEE Trans. Magn.*, *27*, 3433-3443.

Isernia, T., V. Pascazio, and R. Pierri (2001), On the local minima problem in a tomographic imaging technique, *IEEE Trans. Geosci. Remote Sensing, 39,* 1596-1607.

Jones, D. S. (1964), *The Theory of Electromagnetism,* Oxford, U.K.: Pergamon Press.

Kleinman, R. E., and P. M. Van den Berg (1992), A modified gradient method for two-dimensional problems in tomography, *J. Comput. Appl. Math.*, *42*, 17-35.

Liu, Q. H., Z. Q. Zhang, T. T. Wang, J. A. Bryan, G. A. Ybarra, L. W. Nolte, and W. T. Joines (2003), Active microwave imaging 1-2D forward and inverse scattering methods, *IEEE Trans. Microwave Theory Tech.*, *50*, 123-133.

Louis, K. (1992), Medical imaging: state of the art and future development, *Inverse Problems, 8*, 709-738.

Marklein, R., K. Balasubramanian, A. Quing, and K. J. Lagenberg (2001), Linear and nonlinear iterative scalar inversion of multi-frequency mulit-bistatic experimental electromagnetic scattering data, *Inverse Problems*, *17*, 1565-1702.

Massa, A. (2002), Genetic algorithm based techniques for 2D microwave inverse scattering, in *Recent Research Developments in Microwave Theory and Techniques*, Ed. S. G. Pandalai, Transworld Research Network Press, Trivandrum, India.

Miller, E. L., and A. S. Willsky (1996a), A multiscale, statistically based inversion scheme for linearized inverse scattering problems, *IEEE Trans. Geosci. Remote Sensing*, *34*, 346-357.

Miller, E. L., and A. S. Willsky (1996b), Wavelet-based methods for nonlinear inverse scattering problem using the extended Born approximation, *Radio Sci.*, *31*, 51-65.

Natterer, F. (1986), Numerical treatment of ill-posed problems, in *Inverse Problems*, Ed. G. Talenti, *Lecture Notes in Mathematics*, p. 1225.

Richmond, J. H. (1965), Scattering by a dielectric cylinder of arbitrary cross section shape, *IEEE Trans. Antennas Propagat.*, *13*, 334-341.

Steinberg, B. D. (1991), *Microwave imaging techniques,* New York: Wiley.

Testorf, M., and M. Fiddy (2001), Imaging from real scattered field data using a linear spectral estimation techniques, *Inverse Problems*, *17*, 1565-1702.

Vogel, C. R. (2002), *Computational Methods for Inverse Problems*, Philadelphia, PA: SIAM.

Figure Captions

- **Figure 1.** Geometry of the problem.

- **Figure 2.** Numerical Experiments: (a) off-centered homogeneous circular cylinder (Real dataset "Marseille" [*Belkebir and Saillard*, 2001] - "*dielTM_ dec8f.exp*"), (b) two homogeneous circular cylinders (Real dataset "Marseille" [*Belkebir and Saillard*, 2001] - "*twodielTM_ 8f.exp*"), and (c) U-shaped metallic cylinder (Real dataset "Marseille" [*Belkebir and Saillard*, 2001] - "*uTM_ shaped.exp*").

- **Figure 3.** Comparisons between the incident field measured in D_M and the values synthesized by means of the *PW-Model* ((a) amplitude and (b) phase), and *CCW-Model* ((c) amplitude and (d) phase).

- **Figure 4**. Reconstructions of an off-centered homogeneous circular cylinder (Real dataset "Marseille" [*Belkebir and Saillard*, 2001] - "*dielTM_ dec8f.exp*") achieved at the convergence step of the inversion procedure by modeling the radiated field through (a) the single *PW-Model* and (b) the single *CCW-Model*.

- **Figure 5.** Fitting between computed and measured values of the radiated field in the observation domain versus various numbers of source coefficients, S, and for different source models.

- **Figure 6.** Behavior of weighting source coefficients as a function of the index w for (a) the *PW-Model* ($S = 20$) and for (b) the *CCW-Model* ($S = 11$).

- **Figure 7.** Plots of the radiated fields ($V = 1$) computed by means of the *PW-Model* ($S = 20$) (amplitude (a) and phase (b) distributions), the *CCW-Model* ($S = 11$) (amplitude (c) and phase (d) distributions), and the single *CCW-Model* ($S = 1$) (amplitude (e) and phase (f) distributions).

- **Figure 8.** Reconstructions of an off-centered homogeneous circular cylinder (Real dataset "Marseille" [*Belkebir and Saillard*, 2001] - "*dielTM_ dec8f.exp*") achieved at the convergence step of the inversion procedure by modeling the radiated field through (a) the *PW-Model* ($S = 20$) and (b) the *CCW-Model* ($S = 11$).

- **Figure 9.** Normalized behavior of the singular values of $[\mathcal{G}]$ for (a) the *PW-Model* $(S = 20)$ and for (b) the *CCW-Model* $(S = 11)$.

- **Figure 10.** Radiated-field modeling: *DCW-Model* $(S = 15)$. (a) Behavior of weighting source coefficients as a function of the index w. Comparison between the incident field measured in D_M and the numerically-computed values ((b) amplitude and (c) phase).

- **Figure 11.** Plots of the radiated field $(V = 1)$ computed by means of the *DCW-Model* $(S = 15)$ (amplitude (e) and phase (f) distributions).

- **Figure 12.** Reconstruction of an off-centered homogeneous circular cylinder (Real dataset "Marseille" [*Belkebir and Saillard*, 2001] - "*dielTM_dec8f.exp*") achieved at (a) i=1, $(\boldsymbol{b})$ i=2 and (c) at the convergence step (i=3) of the inversion procedure by modeling the radiated field through the *DCW-Model* $(S = 15)$.

- **Figure 13.** Reconstructions of two homogeneous circular cylinders (Real dataset "Marseille" [*Belkebir and Saillard*, 2001] - "*twodielTM_8f.exp*") achieved at the convergence step of the inversion procedure by modeling the radiated field through (a) the single *PW-Model*, (b) the single *CCW-Model* and the *DCW-Model* $(S = 15)$ [(c) real part and (d) imaginary part].

- **Figure 14.** Reconstruction of an U-shaped metallic cylinder (Real dataset "Marseille" [*Belkebir and Saillard*, 2001] - "*uTM_shaped.exp*") achieved at the convergence step of the inversion procedure by modeling the radiated field through the *DCW-Model* $(S = 15)$.

Table Captions

- **Table I.** Reconstruction of an off-centered homogeneous circular cylinder (Real dataset "Marseille" [*Belkebir and Saillard*, 2001] - "*dielTM_ dec8f.exp*") - Estimated geometrical parameters.

- **Table II.** Reconstruction of an off-centered homogeneous circular cylinder (Real dataset "Marseille" [*Belkebir and Saillard*, 2001] - "*dielTM_ dec8f.exp*") - Error figures.

- **Table III.** Reconstruction of an off-centered homogeneous circular cylinder ($SNR = 20\,dB$) for different illuminations and considering various electromagnetic sources - Quantitative error figures [(a) ξ_{tot} , (b) ξ_{int} and (c) ξ_{ext}].

- **Table IV.** Reconstruction of two homogeneous circular cylinders (Real dataset "Marseille" [*Belkebir and Saillard*, 2001] - "*twodielTM_ 8f.exp*") - Estimated geometrical parameters ($d_{(I_{opt})} = \sqrt{\left\{x_{c_{(I_{opt})}}^{(1)} - x_{c_{(I_{opt})}}^{(2)}\right\}^2 + \left\{y_{c_{(I_{opt})}}^{(1)} - y_{c_{(I_{opt})}}^{(2)}\right\}^2}$).

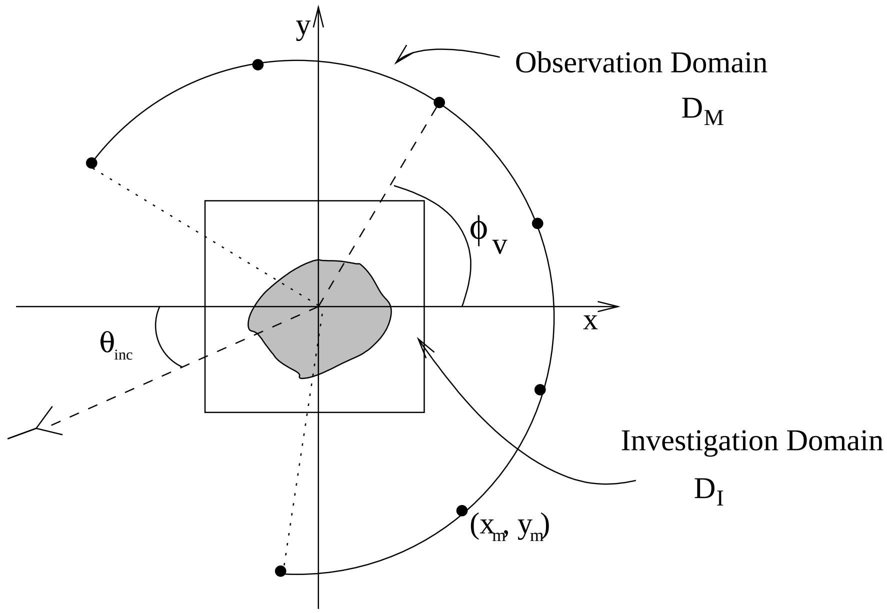

Figure 1 - D. Franceschini *et al.*, "On the Effects of the Electromagnetic..."

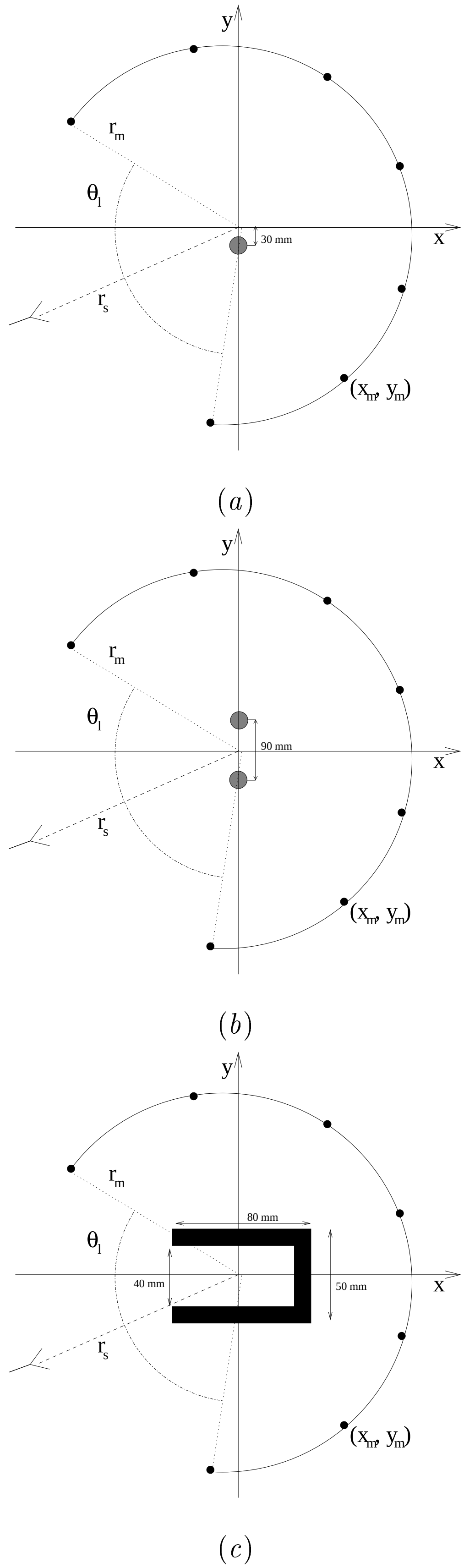

Figure 2 - D. Franceschini *et al.*, "On the Effects of the Electromagnetic..."

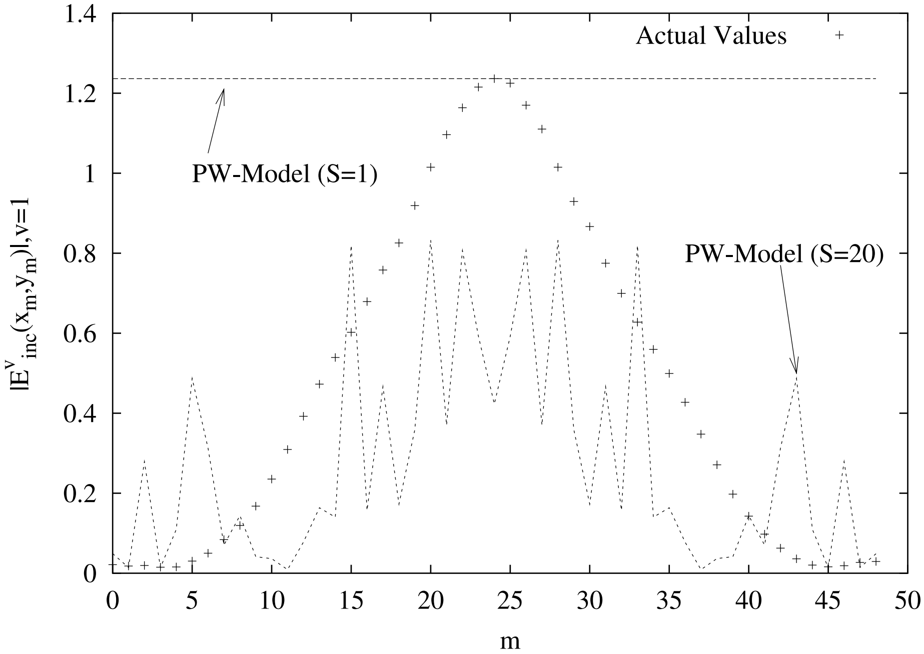

(a)

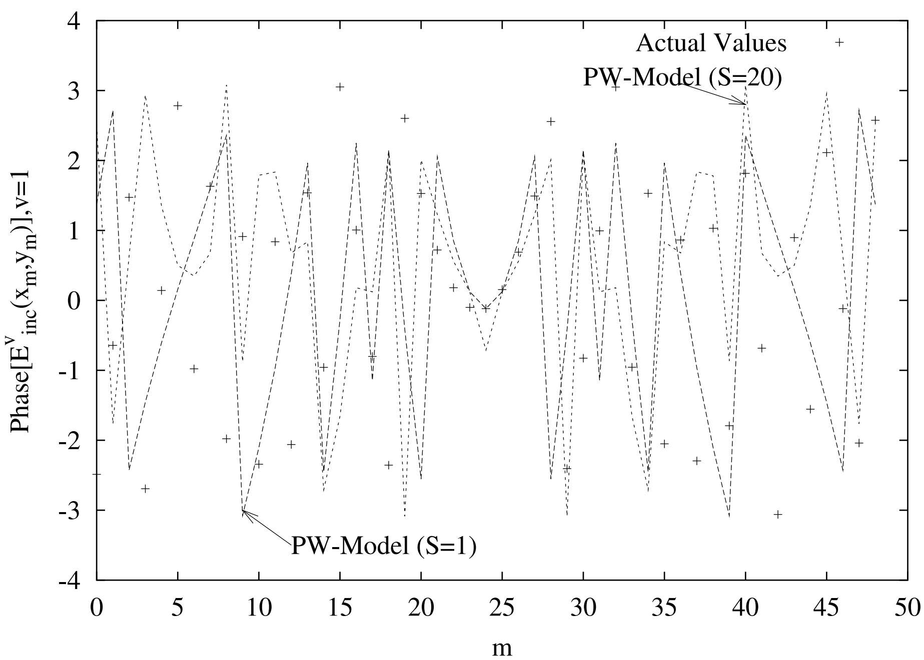

(b)

Figure 3(I) - D. Franceschini *et al.*, "On the Effects of the Electromagnetic..."

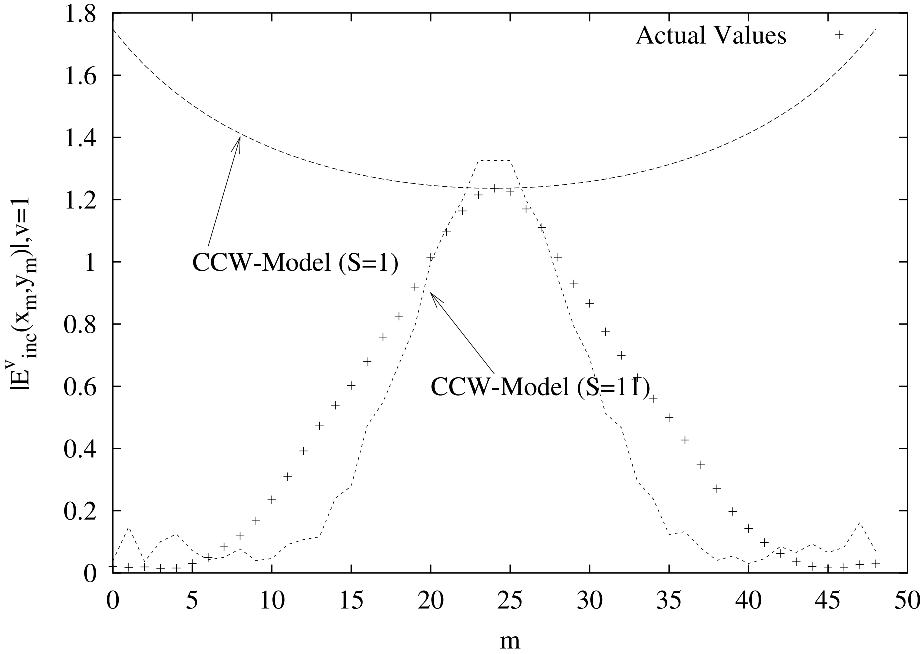

(c)

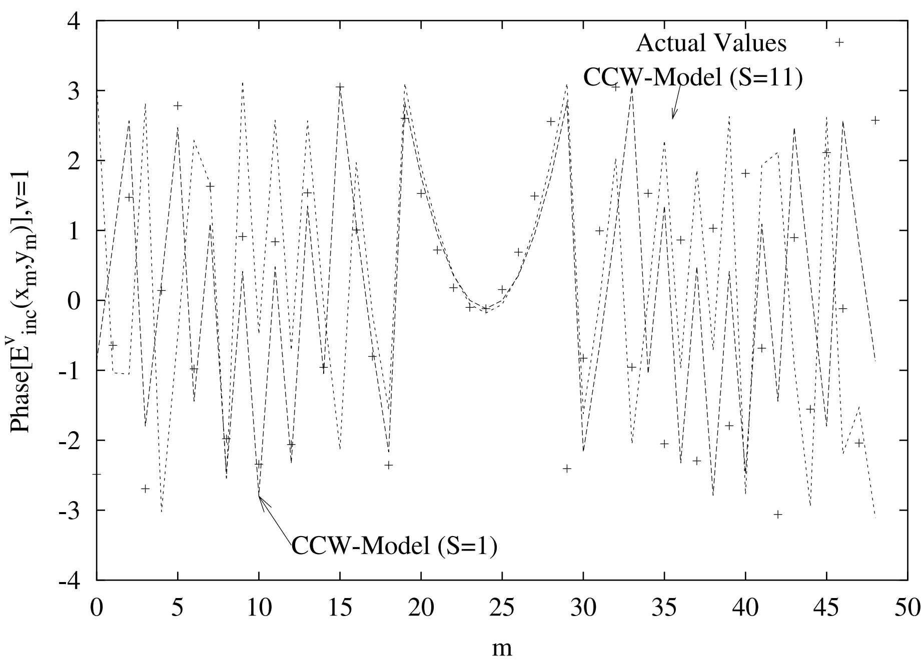

(d)

Figure 3(II) - D. Franceschini *et al.*, "On the Effects of the Electromagnetic..."

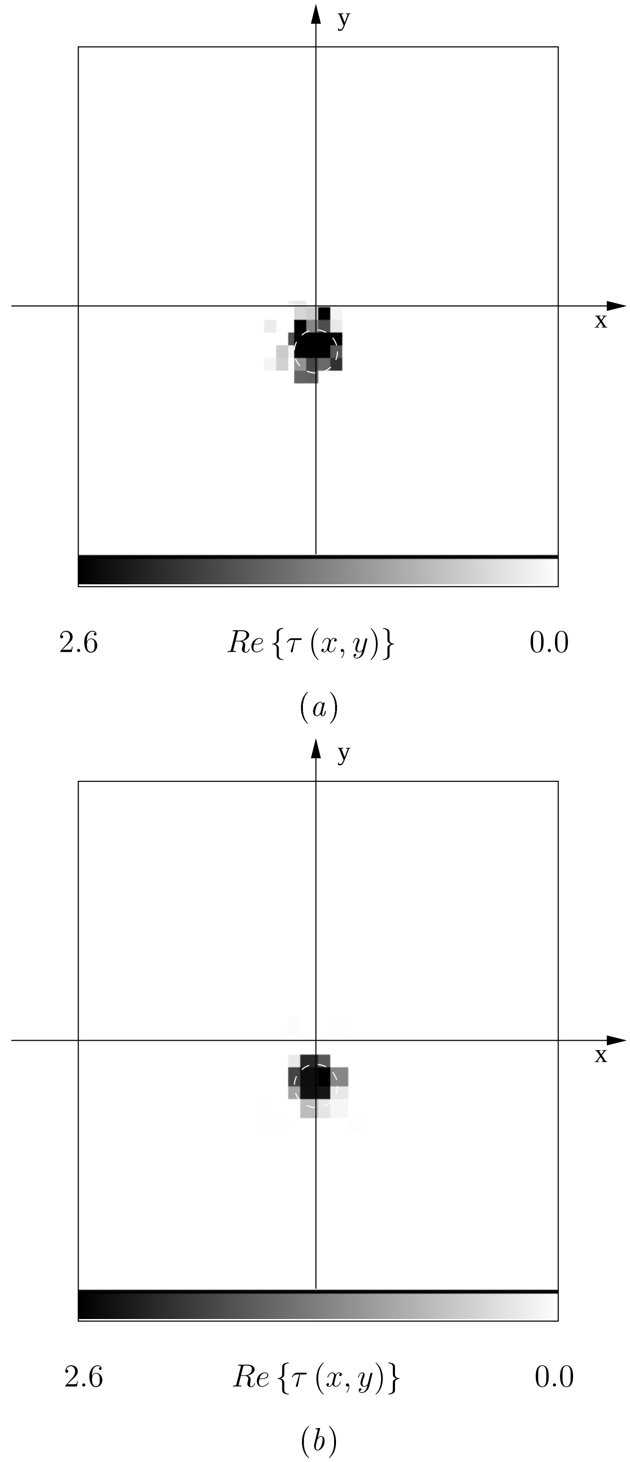

Figure 4 - D. Franceschini *et al.*, "On the Effects of the Electromagnetic..."

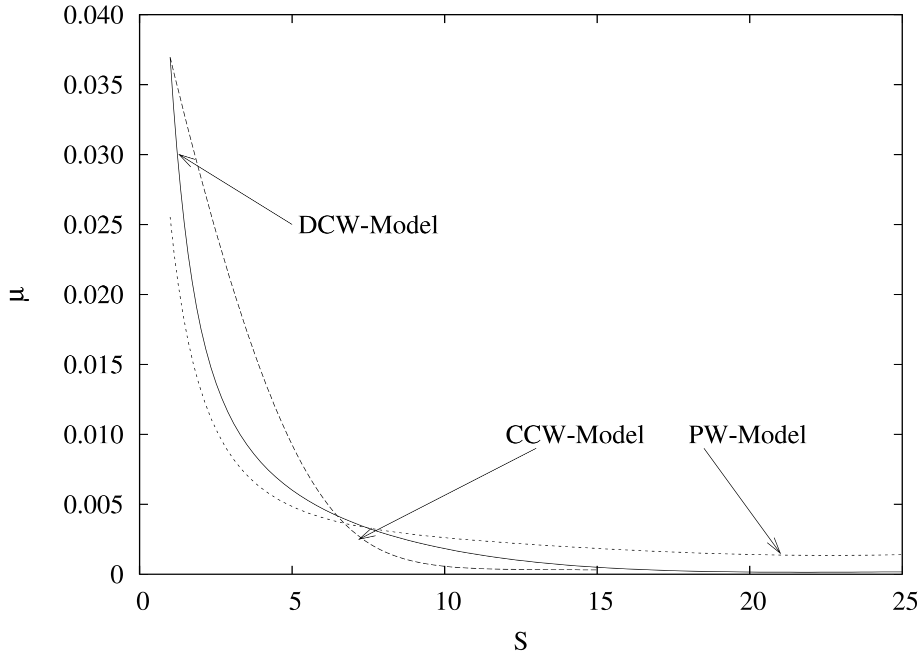

Figure 5 - D. Franceschini *et al.*, "On the Effects of the Electromagnetic..."

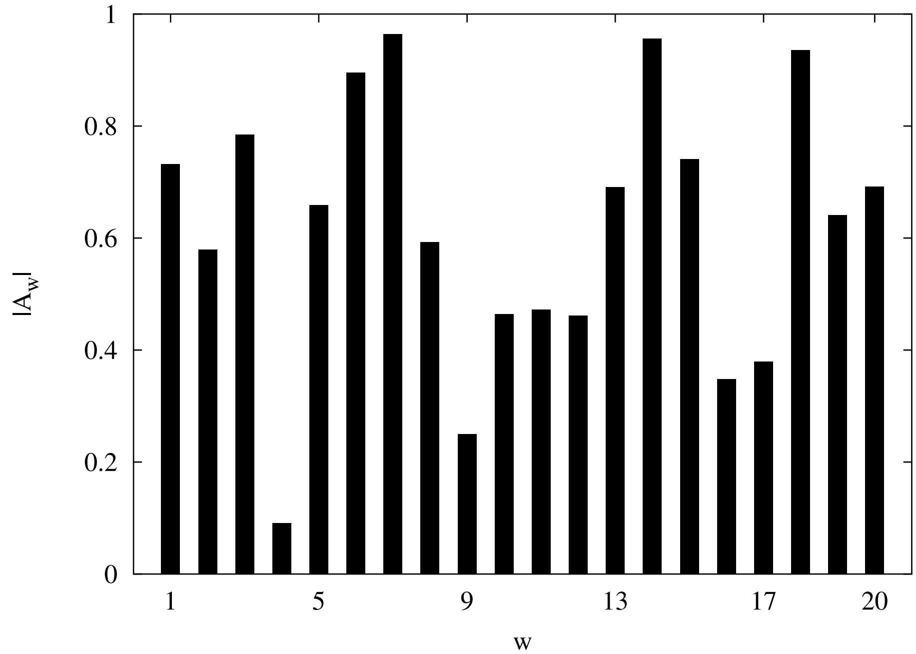

(a)

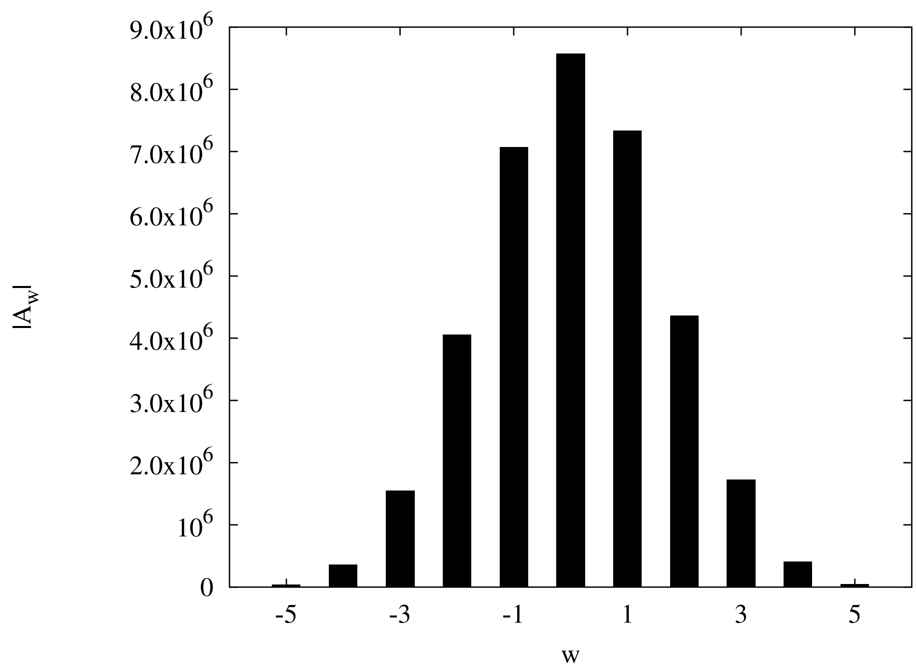

(b)

Figure 6 - D. Franceschini *et al.*, "On the Effects of the Electromagnetic..."

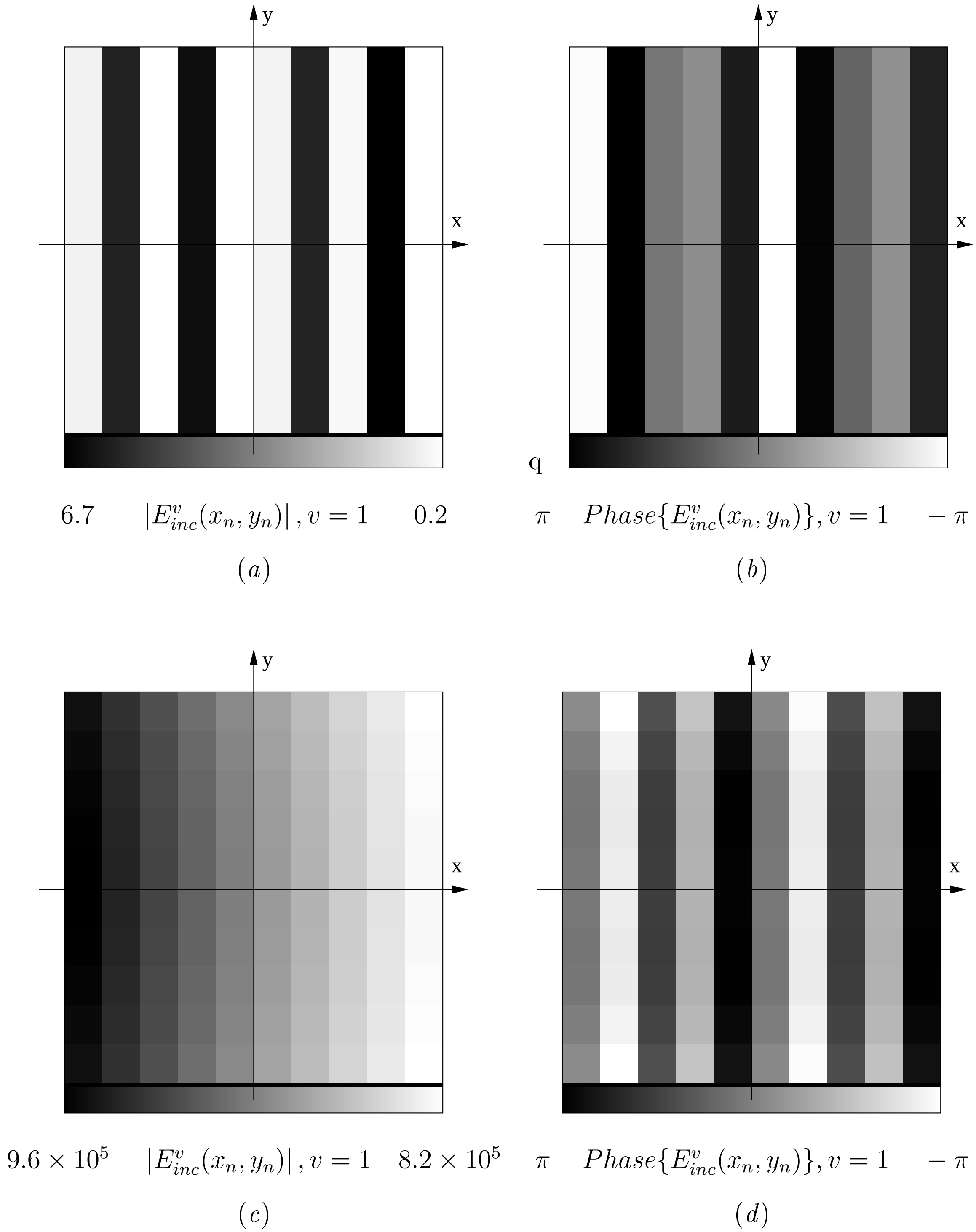

Figure 7(I) - D. Franceschini *et al.*, "On the Effects of the Electromagnetic..."

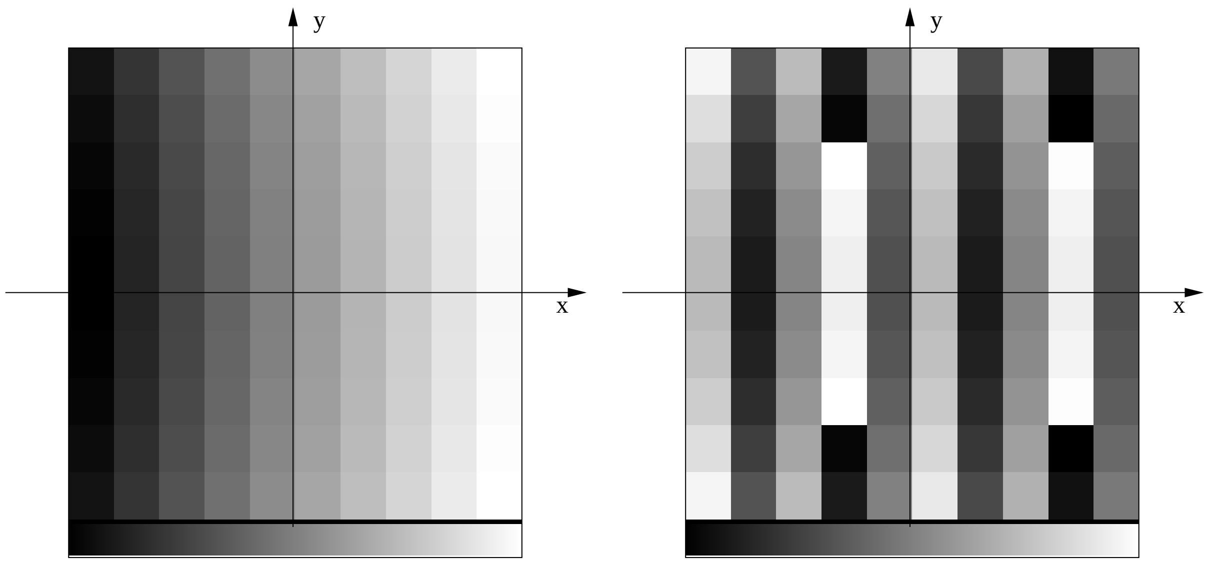

1.97 $\left|E^{v}_{inc}(x_n, y_n)\right|, v = 1$ 1.62 π $Phase\{E^{v}_{inc}(x_n, y_n)\}, v = 1$ $-\pi$

(e) (f)

Figure 7(*II*) - D. Franceschini *et al.*, "On the Effects of the Electromagnetic..."

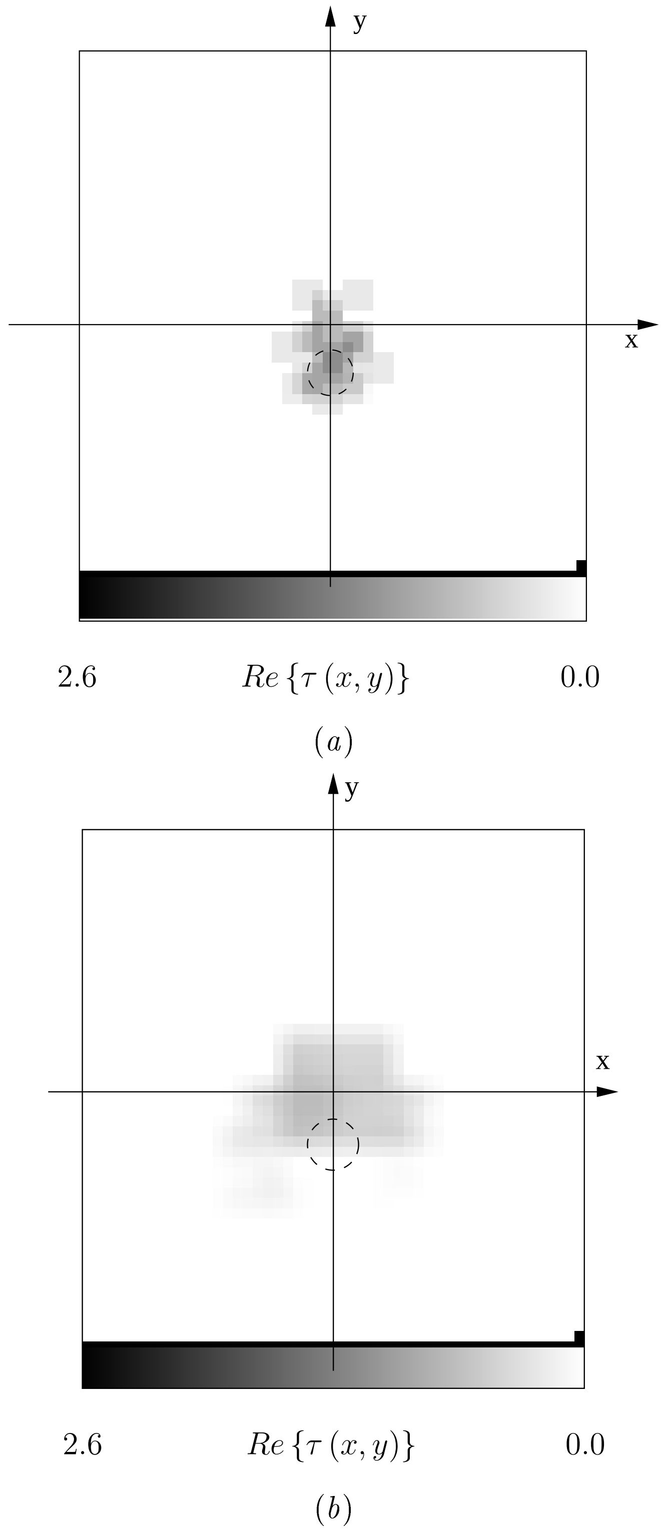

Figure 8 - D. Franceschini *et al.*, "On the Effects of the Electromagnetic..."

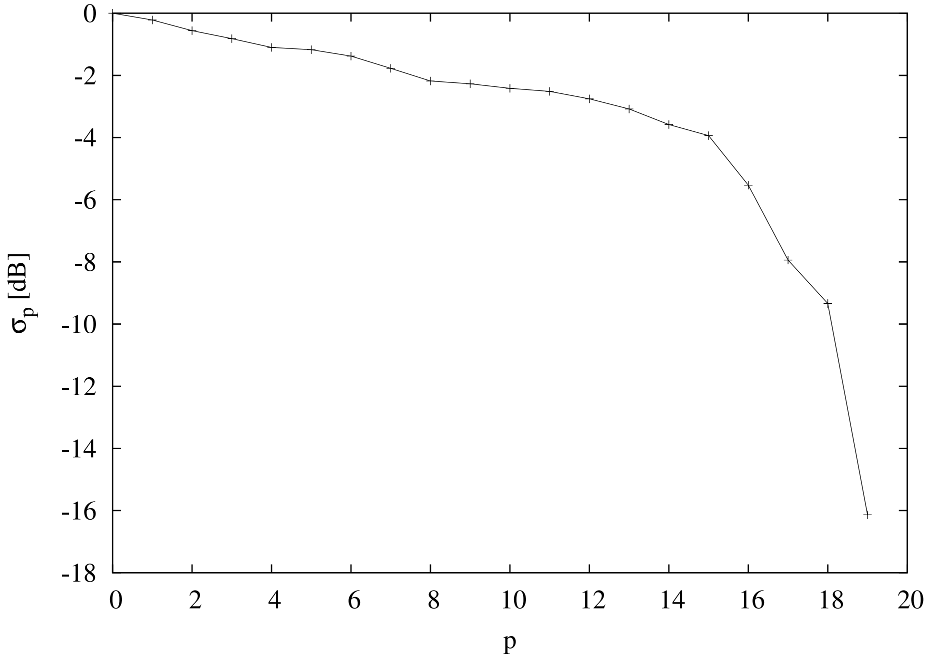

(a)

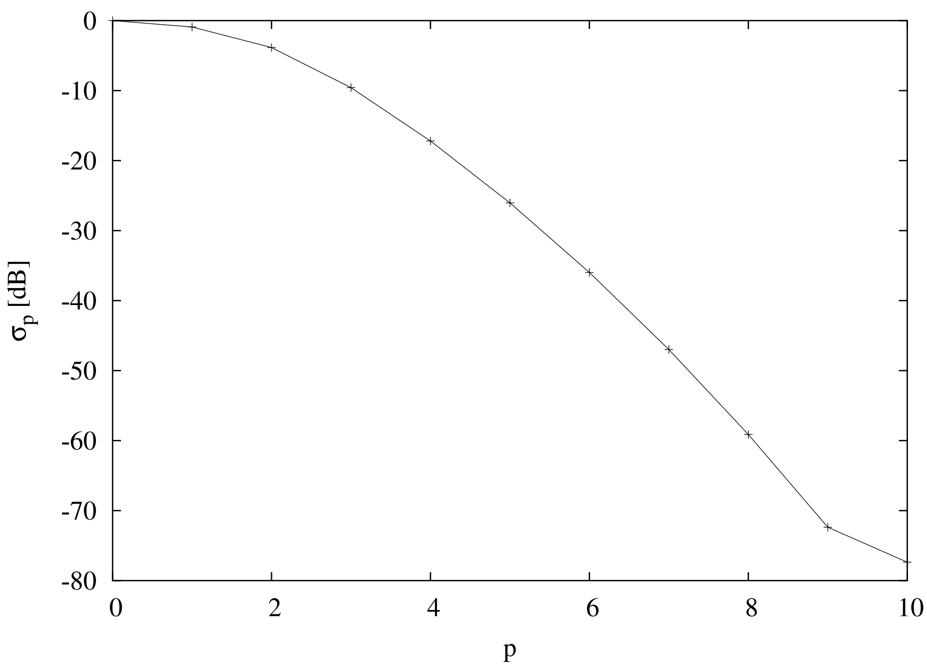

(b)

Figure 9 - D. Franceschini *et al.*, "On the Effects of the Electromagnetic..."

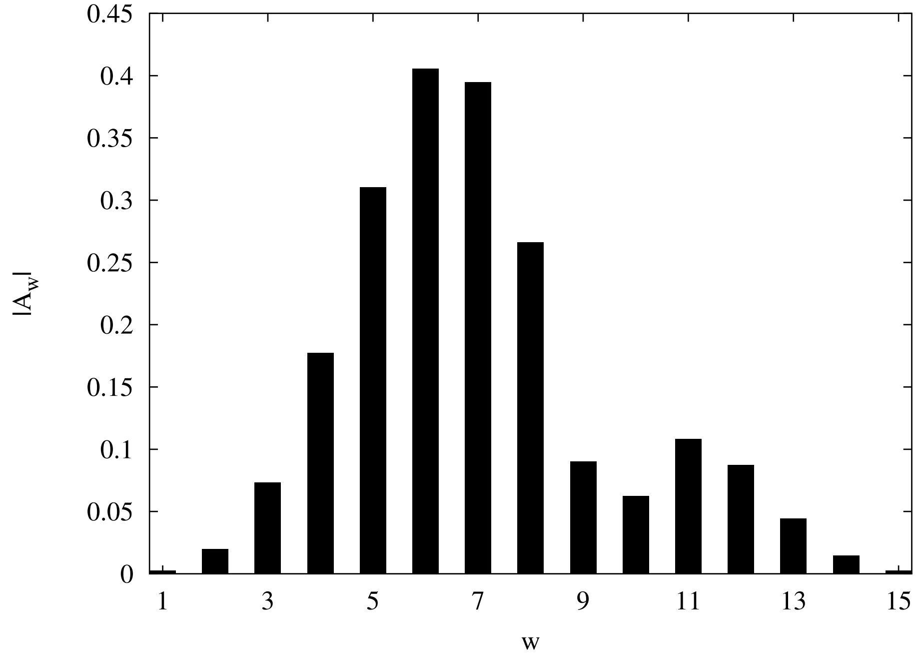

(a)

Figure 10(*I*) - D. Franceschini *et al.*, “On the Effects of the Electromagnetic...”

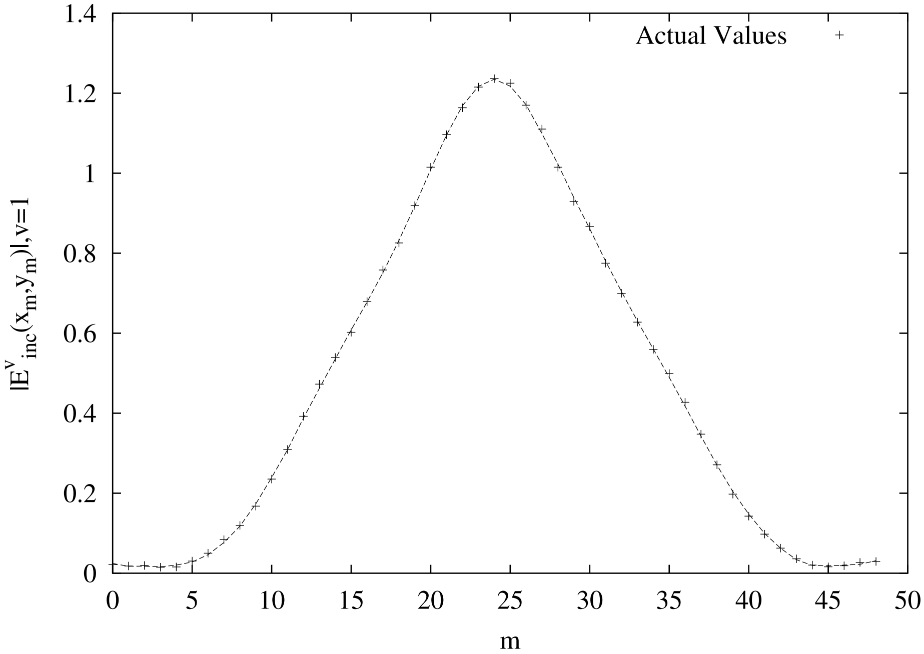

(b)

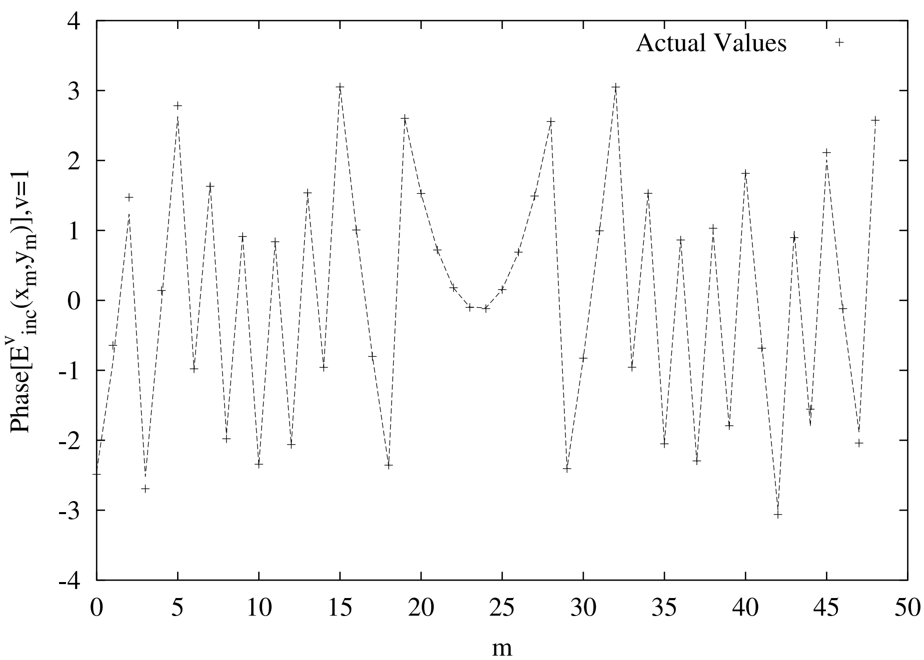

(c)

Figure 10(*II*) - D. Franceschini *et al.*, "On the Effects of the Electromagnetic..."

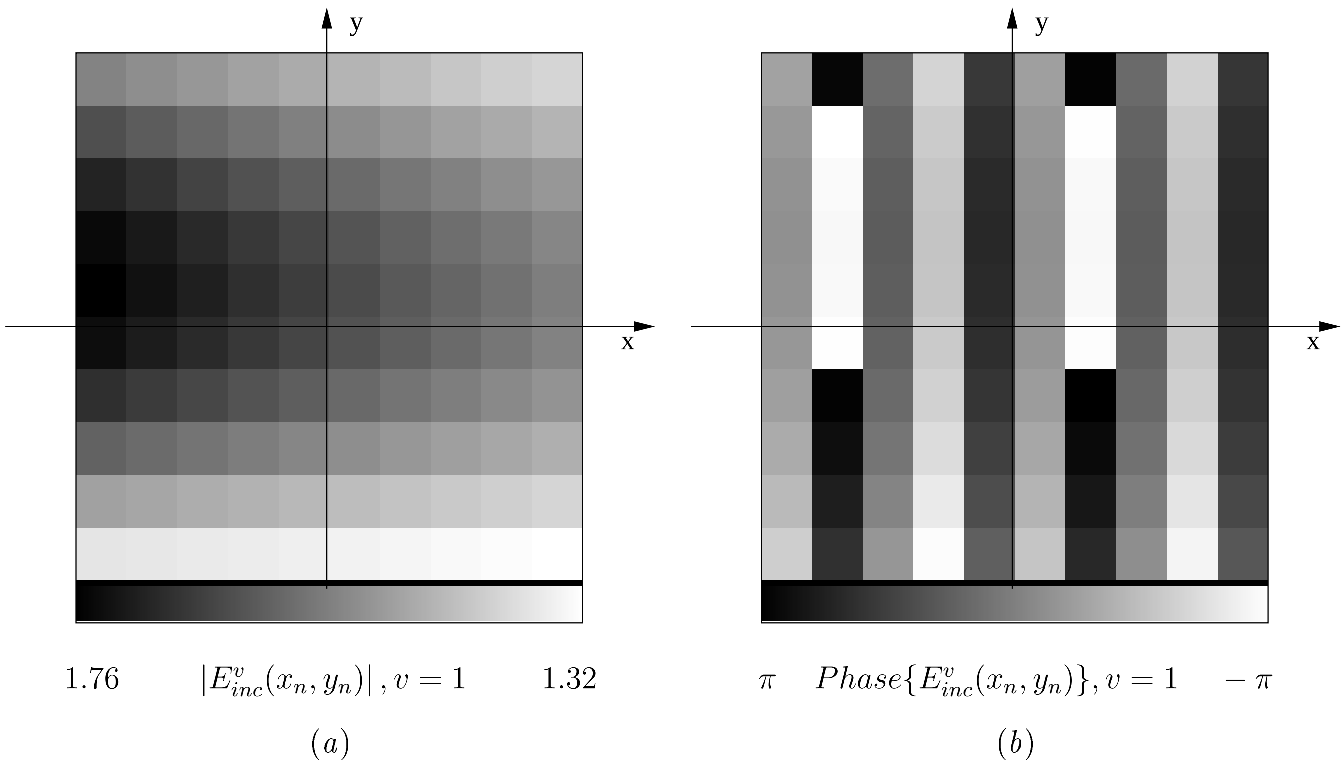

Figure 11 - D. Franceschini *et al.*, "On the Effects of the Electromagnetic..."

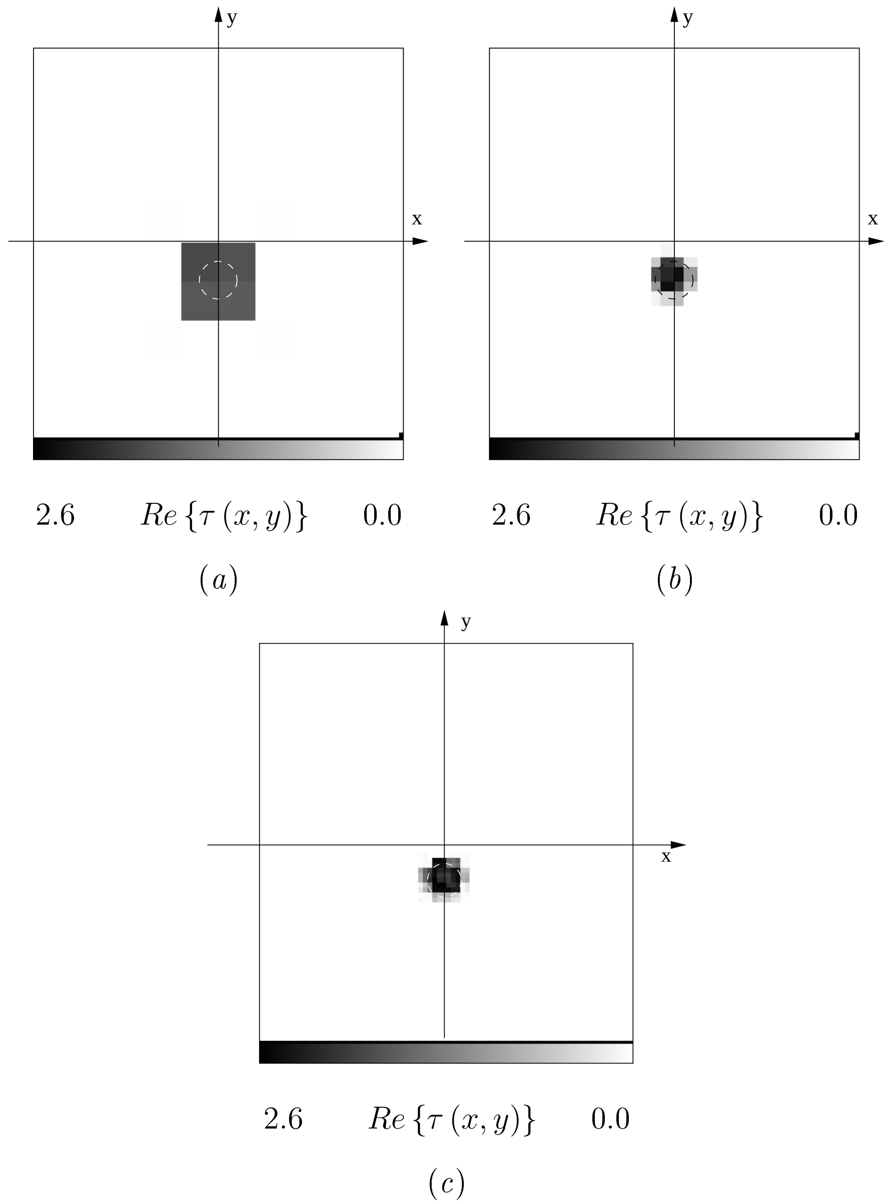

Figure 12 - D. Franceschini *et al.*, "On the Effects of the Electromagnetic..."

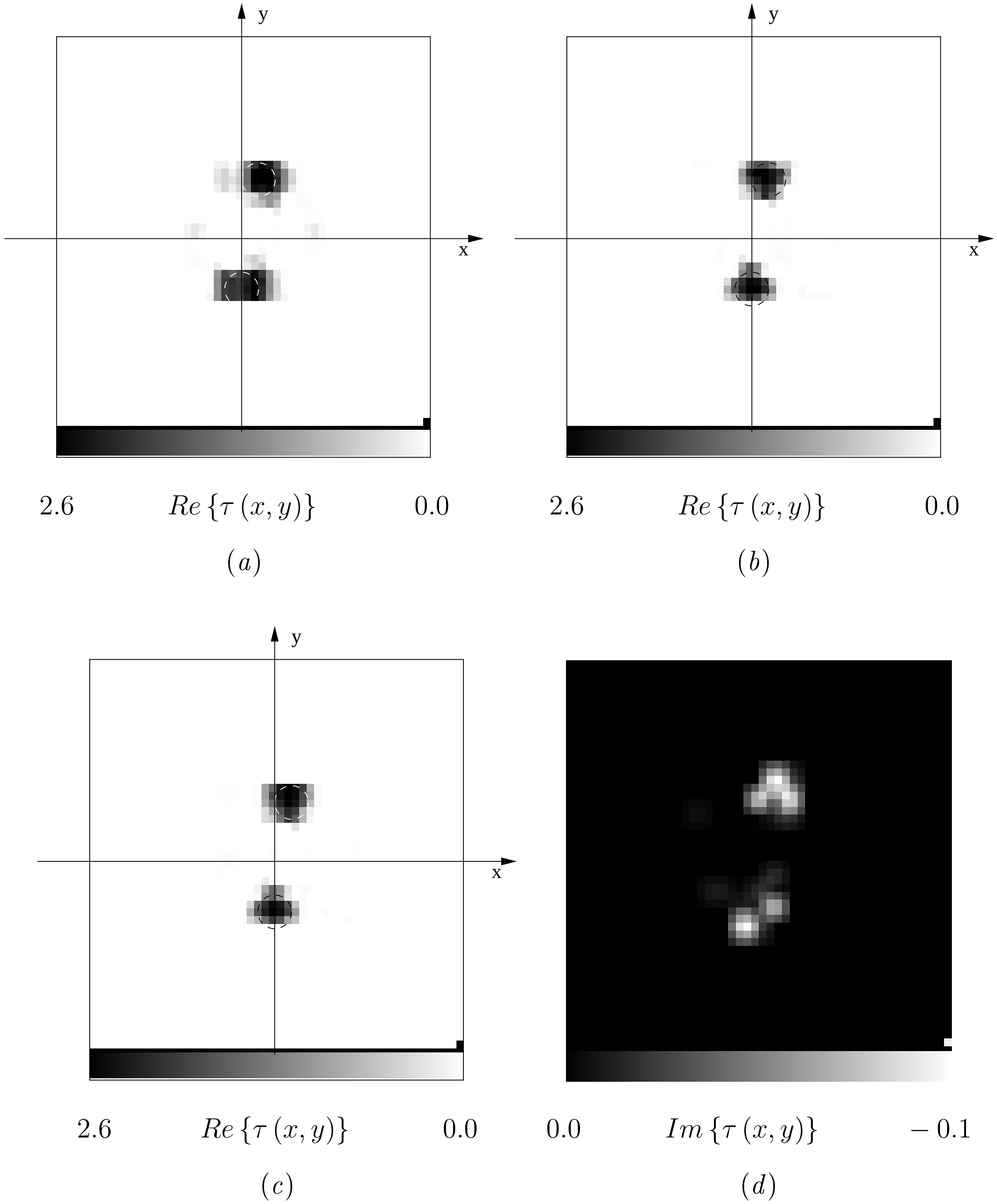

Figure 13 - D. Franceschini *et al.*, "On the Effects of the Electromagnetic..."

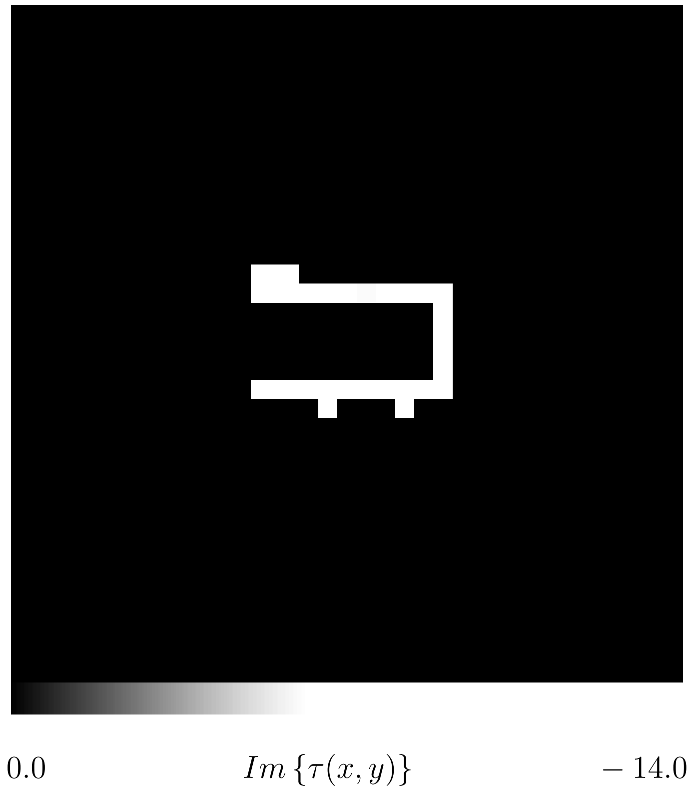

Figure 14 - D. Franceschini *et al.*, "On the Effects of the Electromagnetic..."

	I_{opt}	$x_{c_{(I_{opt})}}$ (mm)	$y_{c_{(I_{opt})}}$ (mm)	$L_{(I_{opt})}$ (mm)
Data Equation Only	4	3.00	−16.00	58.00
PW-Model $(W = S = 1)$	4	−2.00	−26.10	34.00
PW-Model $(W = S = 20)$	4	−2.41	−22.73	45.44
CCW-Model $(W = 0,\ S = 1)$	2	−1.81	−26.10	35.20
CCW-Model $(W = 5,\ S = 11)$	2	1.57	−10.23	60.08
DCW-Model $(W = S = 15)$	3	−1.90	−26.10	27.40

Table I - D. Franceschini *et al.*, "On the Effects of the Electromagnetic..."

	ρ	Δ	$\bar{\tau}$
PW-Model $(W = S = 1)$	0.046	17.3	2.1
CCW-Model $(W = 0, S = 1)$	0.045	13.3	1.7
DCW-Model $(W = S = 15)$	0.045	8.7	1.8

Table II - D. Franceschini *et al.*, "On the Effects of the Electromagnetic..."

ξ_{tot}	***PW-Model***	***CCW-Model***	***DCW-Model***
PW-Source	0.30	20.53	13.30
CCW-Source	16.61	0.37	0.45
DCW-Source	16.44	0.36	0.34

(a)

ξ_{int}	***PW-Model***	***CCW-Model***	***DCW-Model***
PW-Source	13.79	58.64	44.66
CCW-Source	20.31	16.38	17.00
DCW-Source	19.98	25.22	15.29

(b)

ξ_{ext}	***PW-Model***	***CCW-Model***	***DCW-Model***
PW-Source	0.20	19.71	13.06
CCW-Source	16.58	0.25	0.32
DCW-Source	16.42	0.17	0.22

(c)

Table III - D. Franceschini *et al.*, "On the Effects of the Electromagnetic..."

	PW*-*Model ($W = S = 1$)	***CCW*-*Model*** ($W = 0,\ S = 1$)	***DCW*-*Model*** ($W = S = 15$)
$x_{c_{(I_{opt})}}^{(1)}\ (mm)$	12.42	12.89	13.17
$y_{c_{(I_{opt})}}^{(1)}\ (mm)$	40.77	42.96	45.87
$L_{(I_{opt})}^{(1)}\ (mm)$	46.94	40.50	32.70
$x_{c_{(I_{opt})}}^{(2)}\ (mm)$	2.25	2.23	1.88
$y_{c_{(I_{opt})}}^{(2)}\ (mm)$	-45.48	-44.91	-45.27
$L_{(I_{opt})}^{(2)}\ (mm)$	43.70	40.86	32.76
$d_{(I_{opt})}\ (mm)$	86.84	88.50	91.84
I_{opt}	3	3	3

Table IV - D. Franceschini *et al.*, "On the Effects of the Electromagnetic..."